

# Impact of pions on binary neutron star merger

Vimal Vijayan,<sup>1,2,\*</sup> Ninoy Rahman,<sup>1,†</sup> Andreas Bauswein,<sup>1,3,‡</sup>  
Gabriel Martínez-Pinedo,<sup>1,3,4,§</sup> and Ignacio L. Arbina<sup>1,4</sup>

<sup>1</sup>*GSI Helmholtzzentrum für Schwerionenforschung, Planckstraße 1, 64291 Darmstadt, Germany*

<sup>2</sup>*Department of Physics and Astronomy, Ruprecht-Karls-Universität Heidelberg,  
Im Neuenheimer feld 226, 69120 Heidelberg, Germany*

<sup>3</sup>*Helmholtz Forschungsakademie Hessen für FAIR,*

*GSI Helmholtzzentrum für Schwerionenforschung, Planckstr. 1, 64291 Darmstadt, Germany*

<sup>4</sup>*Institut für Kernphysik (Theoriezentrum), Department of Physics,*

*Technische Universität Darmstadt, Schloßgartenstraße 7, 64289 Darmstadt, Germany*

We study the impact of pions in simulations of neutron star mergers and explore the impact on gravitational-wave observables. We model charged and neutral pions as a non-interacting Boson gas with a chosen, constant effective mass. We add the contributions of pions, which can occur as a condensate or as a thermal population, to existing temperature and composition dependent equations of state. Compared to the models without pions, the presence of a pion condensate decreases the characteristic properties of cold, non-rotating neutron stars such as the maximum mass, the radius and the tidal deformability. We conduct relativistic hydrodynamical simulations of neutron star mergers for these modified equations of state models and compare to the original models, which ignore pions. Generally, the inclusion of pions leads to a softening of the equation of state, which is more pronounced for smaller effective pion masses. We find a shift of the dominant postmerger gravitational-wave frequency by up to 150 Hz to higher frequencies and a reduction of the threshold binary mass for prompt black-hole formation by up to  $0.07 M_{\odot}$ . These quantitative changes compared to the equation of state model without pions are stronger for smaller effective pion masses and for underlying baryonic models which result in softer equations of state. We evaluate empirical relations between the threshold mass or the dominant postmerger gravitational-wave frequency and stellar parameters of nonrotating neutron stars. These relations are constructed to extract these stellar properties from merger observations and are built based on large sets of equation of state models which do not include pions. Comparing to our calculations with pions, we find that these empirical relations remain valid to good accuracy, which justifies their use although they neglect a possible impact of pions. Pions simultaneously modify merger characteristics and the properties of cold, nonrotating neutron stars. We also address the mass ejection by neutron star mergers and observe a moderate enhancement of the ejecta mass by a few ten per cent. While such variations may be within statistical uncertainties of the simulations, the increase is slightly more pronounced than one would have expected from empirical relations predicting the ejecta mass based on stellar parameters of nonrotating neutron stars.

## I. INTRODUCTION

The equation of state (EOS) of high-density matter determines the stellar structure of neutron stars (NSs) and the dynamics and outcome of binary neutron star (BNS) mergers. Therefore, the EOS is particularly important to understand the gravitational-wave (GW) emission, nucleosynthesis and electromagnetic radiation of merger events [1–12].

The EOS of neutron star (NS) matter is not fully known and various theoretical models have been put forward along with efforts to obtain insights from observations of, for instance, BNS mergers. The theoretical models are based on different methods to solve the nuclear many-body problem and make different assumptions about the constituents of high-density matter,

e.g. [13–19]. Apart from neutrons, protons and electrons, some models additionally consider for instance hyperons, deconfined quarks, muons, quarks, pions, kaons, and at finite temperatures positrons, photons, neutrinos and anti-neutrinos. The finite-temperature regime of the EOS is relevant for phenomena such as core-collapse supernovae and binary mergers, which can reach temperatures of several 10 MeV (see reviews above).

Already for decades it has been conjectured that negatively charged pions could form a Bose-Einstein condensate in the cores of NSs [20–28]. If and at which density such a condensate occurs, depends on the detailed interactions between pions and nucleons and is currently not known. One expects that pions are associated with an effective pion mass which differs from its vacuum value of about 140 MeV. At finite temperature one may in addition expect that a population of thermal pions is present, where positively and negatively charged pions as well as neutral pions may play a role [29–35].

The influence of pions (either as condensate or thermal population) in BNS mergers is largely unexplored. But see refs [31, 32, 34], which investigate pions in simulations

\* v.vijayan@gsi.de

† n.rahman@gsi.de

‡ a.bauswein@gsi.de

§ g.martinez@gsi.de

of core-collapse supernovae. In fact only a few currently available temperature-dependent EOS tables for astrophysical applications include pions [30, 33, 35, 36]. These calculations indicate a softening of the EOS compared to models without pions, which results from a change of the proton fraction if pions are included.

In this study we provide a first assessment of the potential impact of pions in BNS merger simulations. We adopt a relatively simple model describing pions as a non-interacting Bose gas with a chosen effective mass, and by this consider both condensate and thermal populations of pions. We add the contributions by pions to existing EOS tables and compute the properties of isolated NSs by considering matter in neutrinoless beta-equilibrium at zero temperature. We then focus on the impact in dynamical simulations of BNS mergers and analyze the influence of pions on the dynamics, on black-hole formation, on the GW signal, and on the mass ejection in these events.

A major motivation of this exploration is to evaluate to which extent neglecting pions in previous studies affects empirical relations for the dominant postmerger GW frequency and the threshold mass for prompt black-hole formation, e.g. [37–55]. These relations have been derived from calculations without pions<sup>1</sup> and, partly, they are already employed to interpret observations and to infer EOS information or they may be used in future measurements. We find that most empirical relations also hold for models which include pions although the relations have been built based on calculations that neglect pions. This is because these relations connect properties of isolated, cold, nonrotating NSs with observable properties of the merger. Since the addition of pions modifies both the properties of isolated stars and of the merger, the empirical relations remain to good accuracy unaltered. We find this to hold for different chosen effective pion masses, which supposedly cover a reasonable range and to some extent reflects the more complicated physics of pions in the dense medium of NSs [57–61], which we do not include here. Based on these findings we conclude that it is safe to employ such relations in existing and upcoming studies.

This paper is organized as follows. In Sect. II we describe the inclusion of pions using in existing EOS models which originally do not consider pions. Section III briefly discusses the impact on the stellar structure of isolated, nonrotating stars and provides technical information on the hydrodynamical simulations. Section IV addresses the dynamics of BNS mergers with pions and the detailed analysis of the simulation results including

the GW signal, the threshold binary mass for prompt black-hole formation, and the ejecta. In Sect. V we summarize and discuss the conclusions of our findings. The appendix briefly assess stellar equilibrium models which include also muons and neutrinos in addition to pions.

## II. PIONIC EQUATION OF STATE

In this section, we discuss our procedure of adding pions in an existing non-pionic equation of state (EOS). The tabulated Steiner, Fischer, and Hempel (SFHo) EOS [62–64] and the DD2 EOS [62, 65, 66] are used in this study as base EOSs. These EOSs include neutrons, protons, light nuclei (deuterium, tritium, <sup>3</sup>He, etc.), alpha particles, heavy nuclei (charge number  $Z \geq 6$ ), electrons, and positron as their constituent and assume nuclear statistical equilibrium (NSE) over the whole ranges of density and temperature. The base non-pionic EOSs tabulate various thermodynamic quantities against the baryonic density  $\rho$ , temperature  $T$ , and number fraction of positively charged particles  $Y_p$ . We note that in the absence of pions, the net electron fraction  $Y_e = Y_{e^-} - Y_{e^+}$  is equal to  $Y_p$ , where  $Y_{e^-}$ ,  $Y_{e^+}$  are the number fractions of electrons and positrons, respectively.

The charged pions  $\pi^-$ ,  $\pi^+$  and the neutral pion  $\pi^0$  have vacuum rest masses of  $m_{\pi^\pm} = 139.57039$  MeV and  $m_{\pi^0} = 134.9768$  MeV [67]. We treat pions as a free Bose gas and assume their masses do not change with baryonic density however, see for instance [58, 59, 61, 68] for detailed discussions about the pion mass variation in dense medium). Pions are in thermal and chemical equilibrium with nucleons through the strong interaction. Therefore, the chemical potentials of the pions follow  $\mu_{\pi^\pm} = \mp(\mu_n - \mu_p)$  and  $\mu_{\pi^0} = 0$ , where  $\mu_n$ ,  $\mu_p$ ,  $\mu_{\pi^-}$ ,  $\mu_{\pi^+}$ , and  $\mu_{\pi^0}$  are the chemical potentials of neutrons, protons, negatively charged pions, positively charged pions, and neutral pions, respectively. Since we assume pions are a non-interacting Bose gas, the chemical potential of negatively charged pions should be equal to or smaller than their vacuum rest mass. Additionally, charge neutrality requires  $Y_p = Y_e + Y_\pi = Y_e + Y_{\pi^-} - Y_{\pi^+}$ , where  $Y_\pi$ ,  $Y_{\pi^-}$ , and  $Y_{\pi^+}$  are the net number fraction of charged pions, the number fraction of negatively charged pions, and the number fraction of positively charged pions.

To add charged pions to a base EOS, we apply the following procedure. For a given baryonic density  $\rho$ , temperature  $T$ , and net electron fraction  $Y_e$ , we iteratively determine  $Y_p$  until charge neutrality  $Y_p - Y_\pi = Y_e$  is fulfilled. The base EOS provides  $\hat{\mu} = \mu_n - \mu_p$  and in case  $|\hat{\mu}| < m_{\pi^\pm}$ , the net number fraction of pions  $Y_\pi$  is evaluated employing the Bose-Einstein statistics for a given  $T$  and  $\mu_{\pi^\pm} = \pm\hat{\mu}$  in each iteration.

In neutron-rich conditions when  $Y_p < 0.5$ , the base EOS can yield  $\hat{\mu} > m_{\pi^-}$ . However, the maximum allowed value of negatively charged pions' chemical potential  $\mu_{\pi^-}^{\max}$  is their rest mass as pions are a Bose gas. Under such thermodynamic conditions when  $\hat{\mu} > m_{\pi^-}$ , the

<sup>1</sup> Some of these studies do include a few models with pions such as the APR EOS [36, 56]. However, the majority of employed EOS models ignores pions and thus the models with pions have only a negligible impact on the resulting fits. For simplicity, in the following we will refer to such empirical relations as being obtained from models without pions.

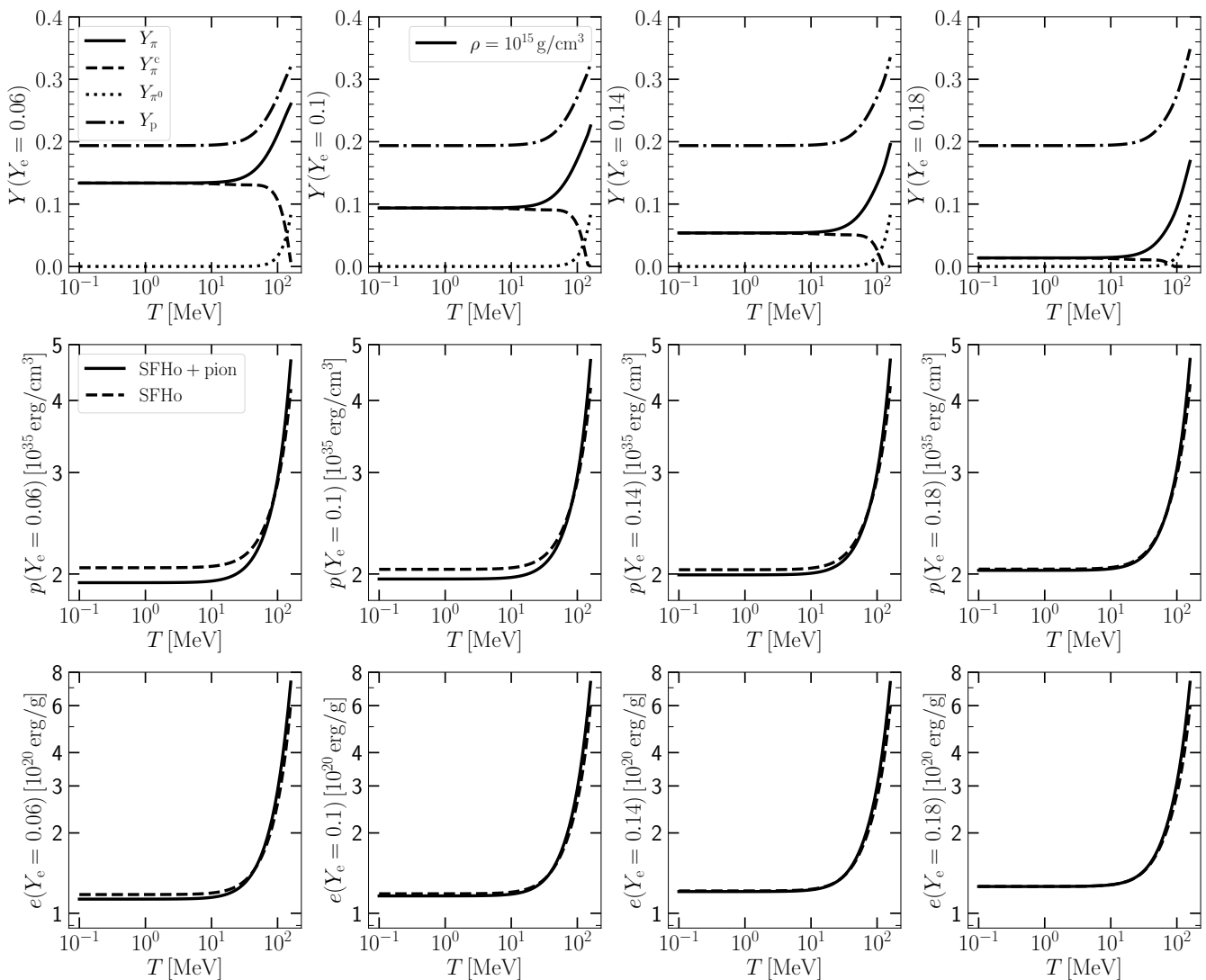


FIG. 1. Comparison between the SFHo EOS and the modified SFHo EOS with pion masses equal to their vacuum values at a baryon density of  $10^{15}$  g/cm $^3$ . The net number fraction of charged pions (solid lines) and number fraction of condensed negative pions (dashed lines), neutral pions (dotted lines), and positive charges (dotted-dashed lines) are shown in the top row. The total pressure and total specific internal energy are shown for the SFHo EOS (dashed lines) and the modified SFHo EOS with pions (solid lines) in the second and third rows, respectively. Different columns represent different electron fractions.

negatively charged pions can form the Bose-Einstein condensate which, unlike thermal pions, have zero kinetic energy. In such conditions, we iteratively solve the equation  $\hat{\mu} = \mu_{\pi^-}^{\text{max}} = m_{\pi^-}$  to find a new value of  $Y_p$  under fixed baryonic density, temperature, and electron fraction. Afterwards, we employ the charge neutrality condition to obtain the number fraction of negatively charged condensed pions  $Y_{\pi^c} = Y_p - Y_e - Y_{\pi^{\text{thermal}}}$  where the number fraction of thermal pions  $Y_{\pi^{\text{thermal}}}$  is evaluated from the Bose-Einstein statistics with  $\mu_{\pi^-} = m_{\pi^-}$ .

This condensed part of  $\pi^-$  does not contribute to the total pressure and the total thermal energy. In proton-rich conditions, a condensate of positively charged pions can form; however, such scenarios are not expected for zero-temperature  $\beta$ -equilibrium neutron stars (NSs) and hypermassive neutron stars (HMNSs). The number frac-

tion of neutral pions can be evaluated easily since it only depends on the temperature of the Bose gas. Finally, we determine the contribution of pions to the pressure, the internal energy, and the total entropy per baryon using the Bose-Einstein statistics.

We note that the base SFHo and DD2 EOSs employed in this study include the electronic contributions corresponding to  $Y_e = Y_p$  in the total pressure, the total energy, and the total entropy of the gas, and the base EOSs tabulate these thermodynamic quantities against the  $\rho$ ,  $T$ , and  $Y_p$ . Therefore, while building our modified EOSs with pions, which tabulate thermodynamic quantities as a function of the  $\rho$ ,  $T$ , and  $Y_e$  with  $Y_e \neq Y_p$ , we first subtract the electronic contributions corresponding to  $Y_p = Y_e + Y_{\pi}$  from the total pressure, the total energy, and the total entropy, and then we add the electronic

contributions corresponding to  $Y_e$  to the total pressure, the total energy, and the total entropy of the gas.

The base EOS considers the Coulomb interactions between charged particles and includes their contributions to the pressure, the internal energy, and the proton chemical potential. The Coulomb contributions in these mentioned thermodynamic quantities can be different for pions and electrons as the mean separation length between positive charges and pions can be smaller than the mean separation length between positive charges and electrons. Despite that, we do not modify the Coulomb contributions to thermodynamic quantities in this paper, which is a caveat of our scheme. However, at densities relevant for pion production, i.e., densities above the nuclear saturation density, the nuclear contributions dominate over the Coulomb contributions. Therefore, our approximation regarding the Coulomb interactions may have a minor impact on the structure of NSs and the GWs emitted during merger, which are the two main topics of this paper.

In a dense medium, the effective pion mass may vary with the baryon density, temperature, and composition. due to the pion-pion interaction and the pion-nucleon interaction (see, e.g., [58, 59, 61, 68]). Reference [61] has shown a significant increase in the mass of the negatively charged pions at densities above saturation density and zero temperature. However, the behavior at typical temperatures of a few 10 MeV, which is the relevant regime for postmerger remnants, requires further studies. For simplicity, we use fixed pion masses adopting the vacuum mass, 170 MeV, and 200 MeV. To probe the consequences of the effective pion mass variation on various thermodynamic quantities, we construct and study EOSs with different constant pion masses. We assume that neutral and charged pions have the same masses and already remark that positively charged pions are strongly suppressed under the relevant conditions such that we do not expect major effects by a possible mass splitting between negatively and positively charged pions. Our treatment may not capture all intricacies of how the dense medium may change the pion EOS (see, e.g., [57, 60, 61, 69] for discussions about the medium modification of pionic EOSs), however, it provides a simple way to study the probable impact of pion mass variations on binary neutron star (BNS) mergers.

In this paper, we use the following notation: “SFHo” for the base SFHo EOS, “SFHo +  $\pi$ ,  $m_\pi = \text{Vac.mass}$ ”, “SFHo+ $\pi$ ,  $m_\pi = 170 \text{ MeV}$ ”, “SFHo+ $\pi$ ,  $m_\pi = 200 \text{ MeV}$ ” for SFHo based EOSs that include pions with effective pion masses equal to the vacuum mass, 170 MeV and 200 MeV, respectively. A similar notation is used for the models based on DD2.

In Fig. 1, we compare the SFHo EOS and the modified SFHo EOS with pion masses equal to their vacuum values at a baryon density of  $10^{15} \text{ g/cm}^3$ . The top panels show the net number fraction of the charged pions  $Y_\pi$  (solid lines), the number fraction of the condensed negatively charged pions  $Y_\pi^c$  (dashed lines), the neutral pions

$Y_{\pi^0}$  (dotted lines), and the positive charges  $Y_p$  (dotted-dashed lines). The middle and bottom panels show the total pressure and the specific internal energy, respectively, for the SFHo EOS (dashed lines) and the modified SFHo EOS with pion masses equal to their vacuum values (solid lines). The panels show the aforementioned quantities as functions of the gas temperature, and different columns represent different electron fractions, namely  $Y_e = 0.06$  (first column), 0.1 (second column), 0.14 (third column), and 0.18 (fourth column). Such values of the electron fraction and the baryon density of  $10^{15} \text{ g/cm}^3$  are representative of conditions in an HMNS (see, e.g., [45, 70–73]).

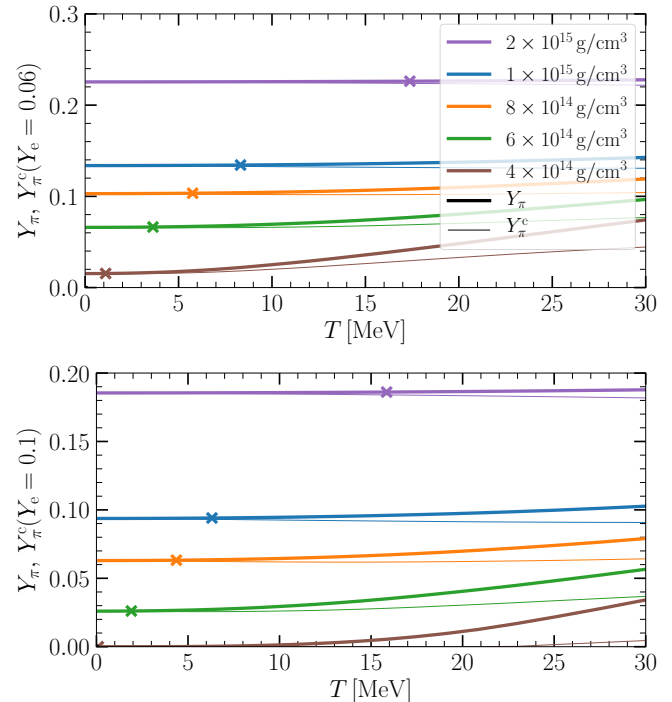


FIG. 2. Net number fraction of charged pions and number fraction of negative pions in the condensate versus temperature at different densities for the modified SFHo EOS with pion masses equal to their vacuum values. The top panel and the bottom panel show these number fractions at electron fractions of 0.06 and 0.1, respectively. The crosses mark the threshold temperatures. We define these threshold temperatures as the points where the number fraction of negative pions in the condensate differs by one percent from the net number fraction of charged pions.

At these thermodynamic conditions, the net number fraction of charged pions and the number fraction of condensed negatively charged pions remain constant below a threshold temperature  $T_{\text{thres}}$ . Below  $T_{\text{thres}}$ , pions are predominately in the Bose-Einstein condensate form ( $Y_\pi \approx Y_\pi^c$ ). As the temperature rises beyond  $T_{\text{thres}}$ , more and more pions go out of the condensate form; moreover, the net number fraction of charged pions grows with the temperature as thermal pions, i.e. pions with non-zero kinetic energies, are produced copiously. We also notice

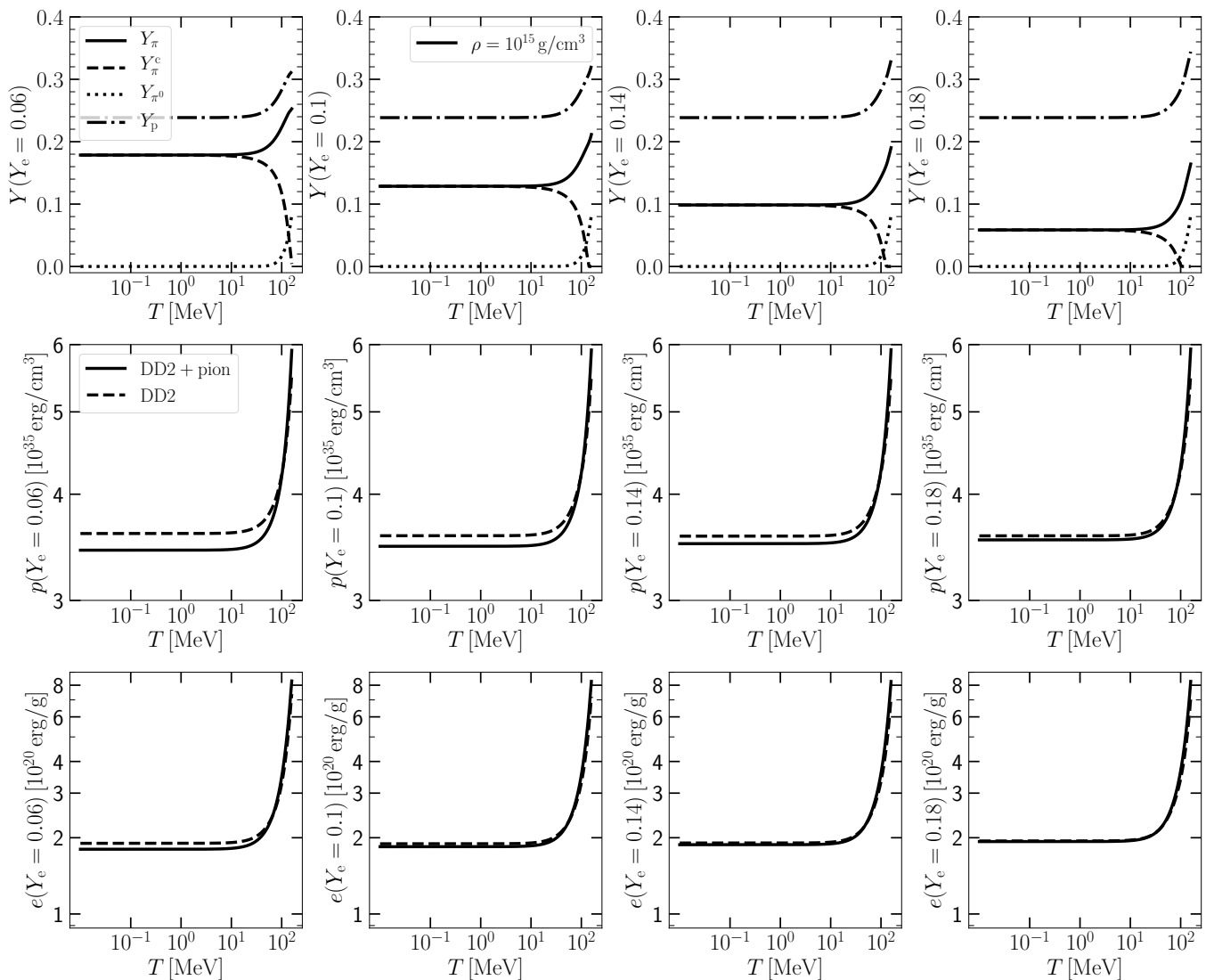


FIG. 3. Comparison between the DD2 EOS and the modified DD2 EOS with pion masses equal to their vacuum values. Quantities shown here are the same as in Fig. 1

that the threshold temperature rises with growing baryon density and diminishes with increasing electron fraction as shown in Fig. 2, where  $T_{\text{thres}}$  are marked by crosses for various densities and electron fractions. We approximate  $T_{\text{thres}}$  as the temperature where the number fraction of condensed negatively charged pions differs by one percent from the net number fraction of charged pions. We also observe that the neutral pions are only produced copiously at high temperatures and their number fraction does not depend significantly on the electron fraction since their chemical potential is zero. In contrast, the net number fraction of charged pions decreases with the growing electron fraction. The number fraction of positively charged particles follows the charge neutrality condition  $Y_p = Y_e + Y_{\pi^+}$ . In neutron-rich conditions shown in Fig. 1, the  $\pi^-$  are more abundant than  $\pi^+$  ( $Y_{\pi^-} > 0$ ) which leads to  $Y_p > Y_e$ ; therefore, the inclusion of pions

production moves baryonic contribution matter towards a more symmetric condition ( $Y_p \rightarrow 0.5$ ) and thus affects the pressure.

The total pressure shown in the middle row of Fig. 1 contains contributions from baryons, electrons, positrons, photons for both EOSs and, in addition, includes contributions from thermal charged pions and the neutral pions for the modified SFHo EOS. The bottom panels of Fig. 1 display the specific internal energy, i.e. the relativistic specific internal energies from which the vacuum rest-mass energies of baryons are subtracted. It contains contributions from baryons, electrons, positrons, photons, and, if present, from pions. The condensed negatively charged pions do not contribute to the pressure as they possess zero kinetic energy and only contribute to the specific internal energies.

At temperatures below several 10 MeV the pressure

as well as the specific internal energy of the EOS which includes pions, is smaller than those of the base EOS. This is because a fraction of the pions exists in condensed form and does not contribute to the thermal pressure and thermal energy. Furthermore, the difference between the two EOSs becomes smaller with increasing electron fraction because of the decreasing net number fraction of charged pions. We also notice that the decrease in the pressure due to pion production is more pronounced compared to that of the specific internal energy.

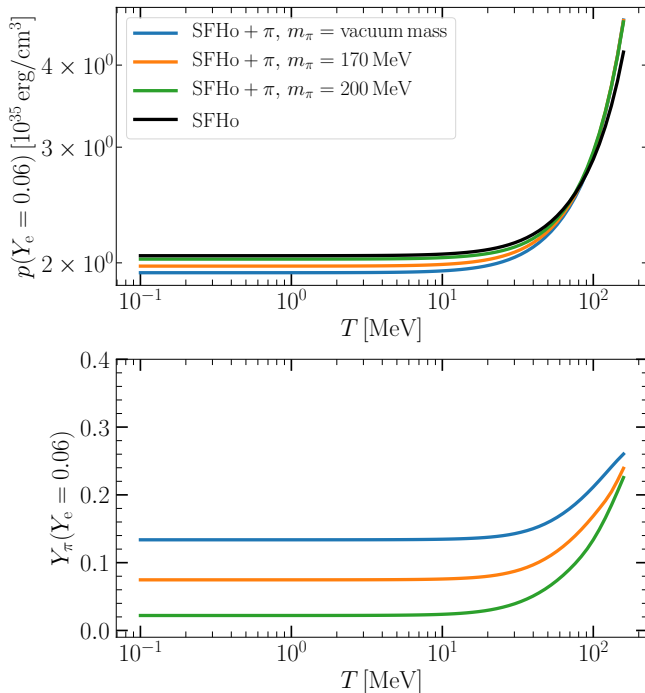


FIG. 4. Total pressure of matter (top panel) and net number fraction of charged pions (bottom panel) versus temperature at a baryon density of  $10^{15}$  g/cm $^3$  and at an electron fraction of 0.06 for the SFHo EOS (black lines) and the modified SFHo EOSs with different pion masses, namely, vacuum mass (blue lines), 170 MeV (orange lines), and 200 MeV (green lines). The total pressure of matter for the modified EOSs with pions converges towards the SFHo EOS values as the mass of the pion increases. Moreover, the net number fraction of charged pions decreases with the growing pion mass.

As temperature rises and pions go out of the condensed form, these reductions in the pressure and the specific internal energy vanish, and at temperatures above several 10 MeV, the pressure and the specific internal energy of the modified SFHo EOS become larger than that of the base SFHo EOS due to the contributions from the thermal charged pions and the neutral pions, which are produced abundantly at high temperature.

In Fig. 3, we show the comparison between the DD2 EOS and the modified DD2 EOS with pion masses equal to their vacuum values. The quantities shown in Fig. 3 are the same as in Fig. 1. The qualitative trends discussed above for the modified SFHo EOS are also ob-

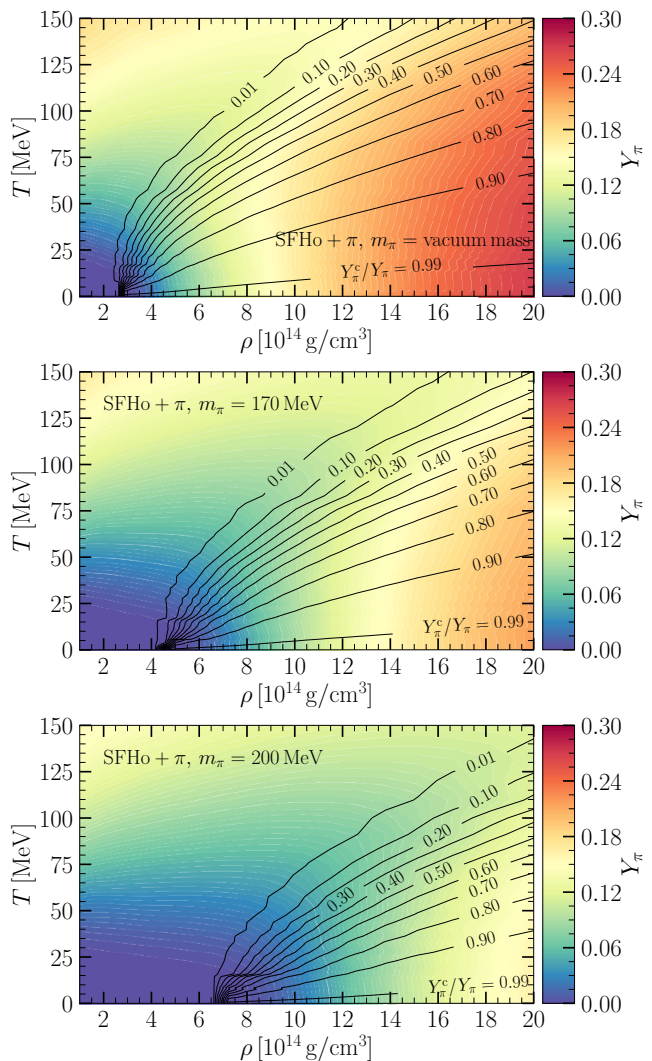


FIG. 5. Equilibrium net number fractions of charged pions, i.e., the net number fraction of charged pions when the charged pions, nucleons, and electrons are in chemical equilibrium, are shown colour-coded on the baryon density-temperature plane ( $\rho$ - $T$  plane) for the modified SFHo EOSs with pion masses equal to their vacuum values (top panel), 170 MeV (middle panel), and 200 MeV (bottom panel). The ratios of the equilibrium number fraction of negatively charged condensed pions and the equilibrium net number fraction of charged pions are marked by black lines.

served for the modified DD2 EOS. However, there are some quantitative differences between the modified DD2 EOS and the modified SFHo EOS, which are expected since the base EOSs are based on different nuclear models [64–66].

In Fig. 4, we depict the total pressures (top panel) and the net number fractions of charged pions (bottom panel), respectively, versus temperature at a baryon density of  $10^{15}$  g/cm $^3$  and an electron fraction of 0.06 for the SFHo EOS (black lines) and the modified SFHo EOS with various pion masses, namely the vacuum masses

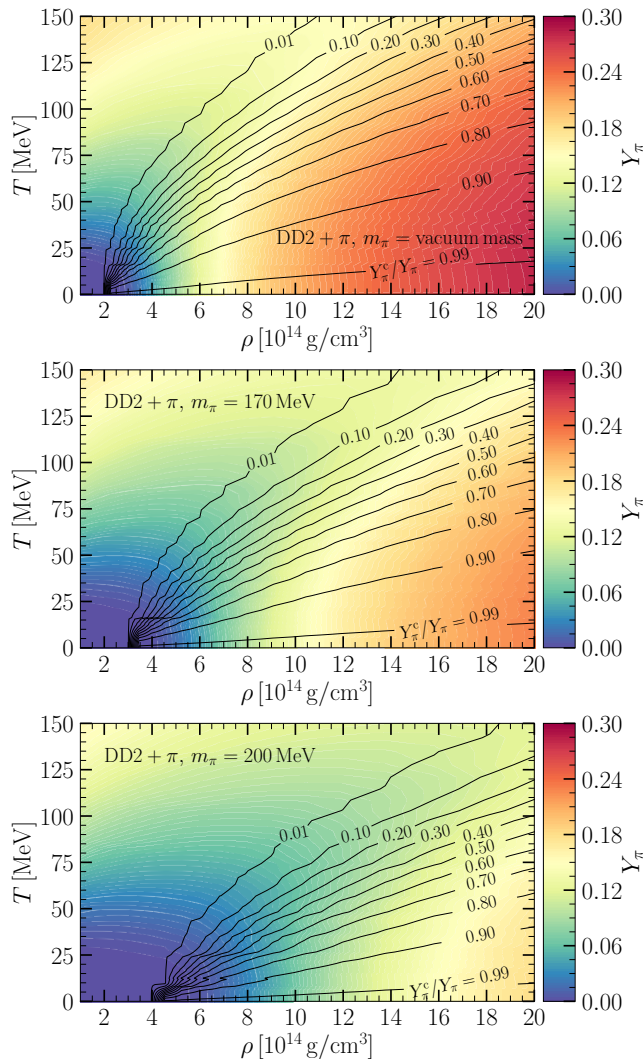


FIG. 6. Same as Fig. 5 but for the EOSs based on the DD2 model.

(blue lines), 170 MeV (orange lines), and 200 MeV (green lines). For large pion masses, the total pressure of the modified SFHo EOSs approaches that of the base EOS. This reduction in the total pressure difference between the modified SFHo EOSs and the base SFHo EOS is expected since the charged pion production diminishes with increasing pion mass. The reduced pion production is reflected by the shift of the net number fraction of charged pions to smaller values as the pion masses increase (lower panel). Recently, [61] discusses the density dependence of pion mass at  $T=0$ . They showed the negatively charged pion mass can be greater than 200 MeV at densities relevant for the pion production, i.e., at densities greater than nuclear saturation density. The net pion fraction will be minuscule for such a high value of negatively charged pion mass and the impact of pion production on the total pressure, the total energy, etc. will be negligible. The dependence of pion effective mass on the den-

sity and temperature and how pion's energy-momentum dispersion relation changes in a dense medium require further studies.

In Fig. 5, we show the net number fraction of charged pions colour-coded on the baryon density-temperature plane ( $\rho$ - $T$  plane) for modified SFHo EOSs with pion masses equal to their vacuum values (top panel), 170 MeV (middle panel), and 200 MeV (bottom panel). Additionally, we mark the ratios of the number fraction of condensed charged pions and the net number fraction of charged pions  $Y_\pi^c/Y_\pi$  by black lines.  $Y_\pi$  and  $Y_\pi^c$  are evaluated under the assumption that the charged pions are in chemical equilibrium with the nucleons and electrons  $\mu_{\pi^-} = \mu_n - \mu_p = \mu_e$ , where  $\mu_e$  is the chemical potential of electrons. The  $Y_\pi^c/Y_\pi = 0.99$  line corresponds to the threshold temperature  $T_{\text{thres}}$  (see also Fig. 2). We notice from Fig. 5 that for a given temperature, the net number fraction of charged pions typically rises with the baryon density; moreover, the ratio between  $Y_\pi^c$  and  $Y_\pi$  increases with the baryon density for all modified EOSs. A larger fraction of negatively charged pions enters the condensed state as the temperature decreases, which is also evident from Figs. 1 and 2. By comparing the panels for different modified SFHo EOSs, i.e. different assumed pion masses, in Fig. 5, we see that the value of  $Y_\pi$  drops with increasing charged pion masses for a given baryon density and temperature. As the charged pion masses grow, a larger density and a lower temperature are needed to achieve the same value of  $Y_\pi^c/Y_\pi$  ratio because a larger value of  $\hat{\mu}$  is required to form the pion condensate. Similar qualitative trends in  $Y_\pi$  and  $Y_\pi^c/Y_\pi$  with varying density, temperature, and pion masses can be observed for the modified DD2 EOSs in Fig. 6.

### III. STELLAR STRUCTURE AND MERGER MODELLING

To understand the impact of pions in BNS mergers, we conduct a number of simulations using the EOSs discussed in section II with effective pion masses equal to their vacuum masses, 170 MeV, and 200 MeV based on the SFHo and DD2 model, respectively. As a reference, we also consider simulations using the base EOSs without pions.

#### A. Stellar structure of isolated NS star

Before we describe merger simulations with the new EOS models, we briefly discuss the impact of pions on the stellar structure by considering the zero temperature<sup>2</sup>

<sup>2</sup> For the sake of simplicity we write “zero temperature” although the lowest temperature listed in the EOS tables is 0.1 MeV, and we compute TOV profiles for this temperature.

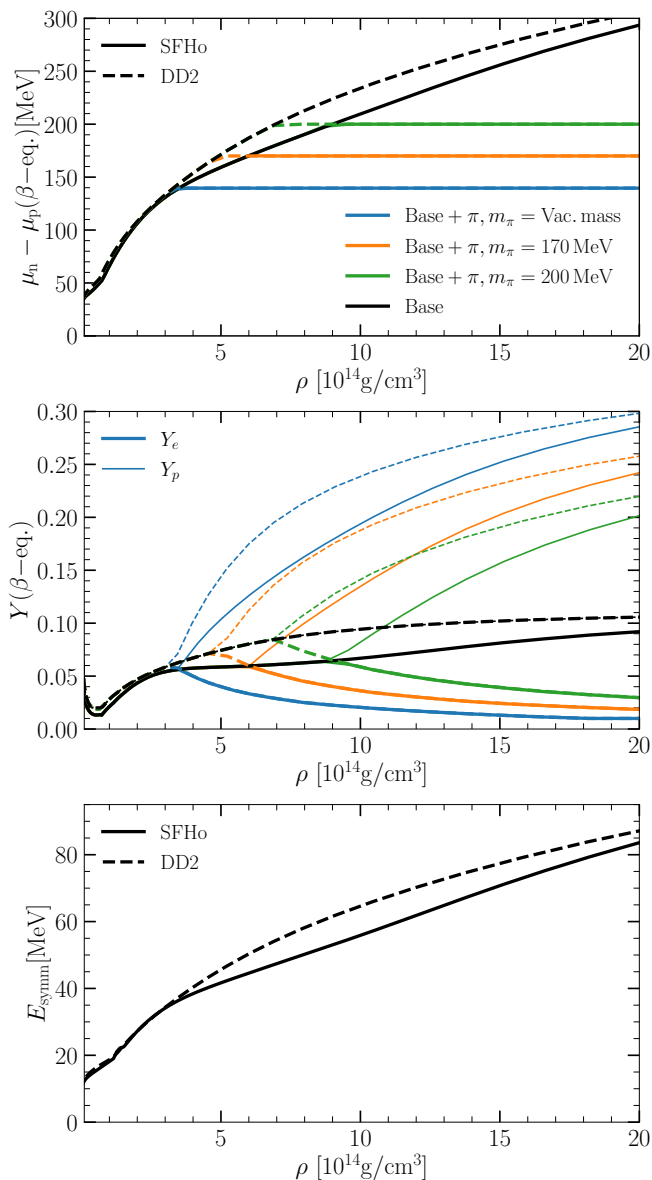


FIG. 7. Top panel shows the difference between neutron and proton chemical potential as function of density at zero temperature for beta-equilibrium. Middle panel provides the electron fraction and proton fraction in beta-equilibrium. Bottom panel displays symmetry energy of nuclear matter as the energy difference between neutron matter and symmetric matter. In all panels black curves refer to the base EOS without pions. Colored curves show the aforementioned quantities for EOSs with pions assuming different effective pion masses. Solid lines are for SFHo based models, while dashed curves visualize DD2 based models. In the middle panel thin lines display the proton fraction and thick lines indicate the electron fraction. For the base models both coincide.

neutrinoless beta-equilibrium slices of the EOS models and by solving the Tolman–Oppenheimer–Volkoff (TOV) solution [74, 75] for these barotropic relations.

Considering pions in NS matter has a strong impact on the conditions for chemical equilibrium, and by this

it affects the stellar structure of NSs in equilibrium. It also determines the initial conditions for binary mergers. The conditions for beta-equilibrium at zero temperature are clarified in Fig. 7. The upper panel shows the difference between the chemical potentials of neutrons and protons as function of density. Once the  $\mu_n - \mu_p$  reaches the effective pion mass, the difference remains constant. Hence, the electron chemical potential is constant, which implies that the electron fraction  $Y_e$  decreases with density because  $\mu_e = \text{const.} \propto n_e^{1/3} \propto (\rho Y_e)^{1/3}$  for relativistic electrons. This can be seen in the middle panel, where the thick lines exhibit  $Y_e$ . Since the electron chemical potential is given by the effective pion mass, the electron fraction is independent of the nuclear EOS in the regime where  $\mu_n - \mu_p$  remains constant. For larger effective pion masses, this behavior sets in at a higher density. Also, at this threshold density the proton fraction starts to deviate from the electron fraction (middle panel) because of the occurrence of condensed pions. In comparison to the base EoS,  $Y_p$  is increased and charge neutrality is established between protons, electrons and pions.

The proton fraction does show a dependence on the nuclear EOS at all densities, i.e. also in the regime with pion condensation. Hence, the fraction of pions does also depend on the EOS fulfilling charge neutrality.

This behavior can be understood by considering the symmetry energy of the EOS defined as the energy difference between neutron matter and symmetric matter. The symmetry energy is known to determine the proton fraction in beta-equilibrium for matter composed of neutrons, protons and electrons by connecting the difference of chemical potentials between neutrons and protons,  $\hat{\mu} = \mu_n - \mu_p$ , and  $Y_p$  (see e.g. [76, 77]; noting that slightly different definitions of the symmetry energy are used in the literature). In the regime of pion condensation with  $\hat{\mu} = \text{const.}$ , the proton fraction is thus entirely determined by the symmetry energy. The symmetry energy is given in the bottom panel of Fig. 7. As the symmetry energy increases for constant  $\hat{\mu}$ , the proton fraction increases, which is clearly visible in the middle panel. The middle panel also shows that the proton fraction is larger for the DD2 based models, which is a consequence of their larger symmetry energy (bottom panel).

In Fig. 8(a), we show the NS gravitational masses versus central densities (top panel) and NS radii (bottom panel) at zero temperature for the SFHo EOS and the modified SFHo EOSs with pions, respectively. Figure. 8(b) displays the same relations for the DD2 EOS and modified DD2 EOSs, respectively. The production of condensed pions in a NS lowers the pressure support against gravity and leads to a reduced mass for the same central density as we can notice from the top panel of Figs. 8(a) and 8(b). The maximum mass is also reduced by the inclusion of pions for both EOS models. The effect amounts to at most one to two percent for the models adopting the vacuum masses. For higher effective pion masses the impact is smaller. See Tabs. I and II. Similar trends are found for NS radii, which are reduced by about

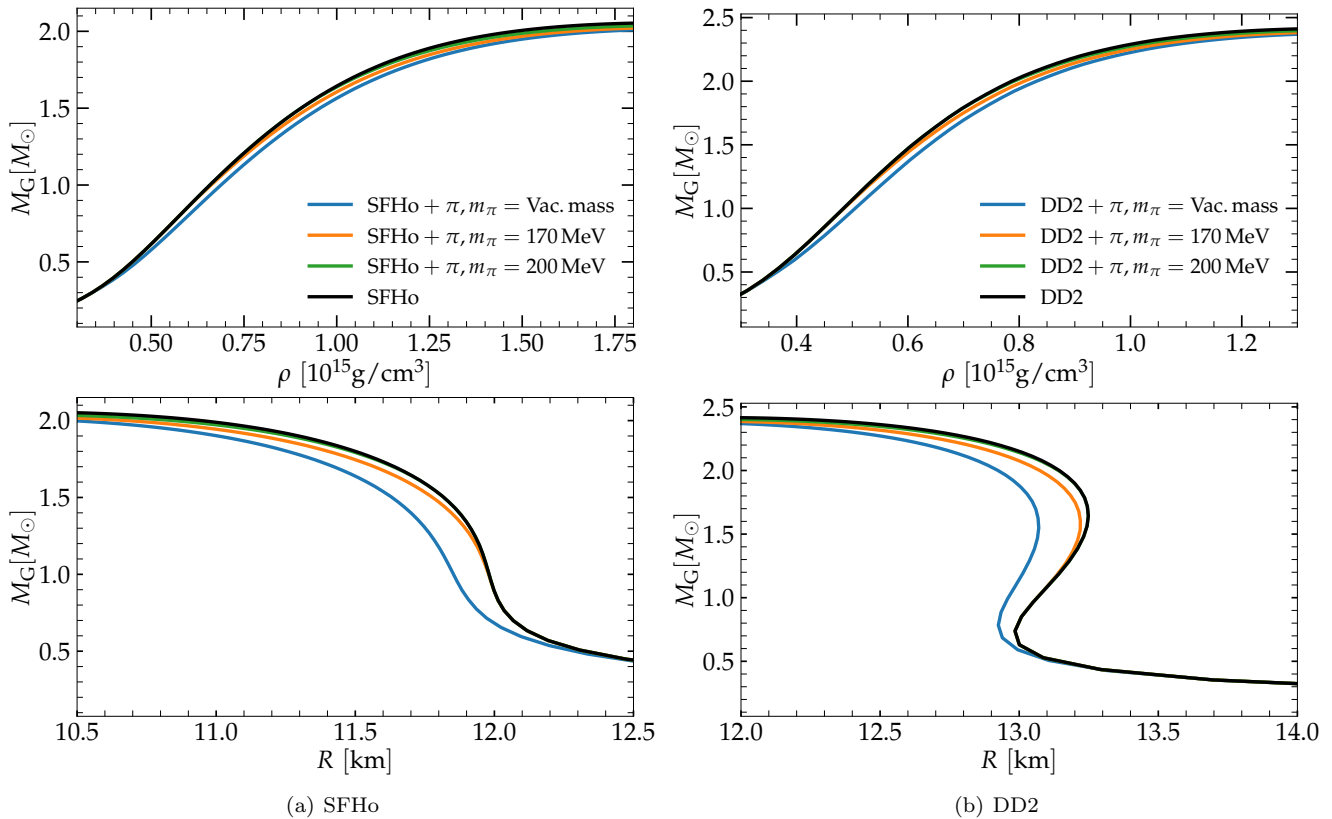


FIG. 8. Left: Gravitational mass versus central baryon density (top panels) and gravitational mass versus the radius of NSs (bottom panels) for the base SFHo EOS and the ones including pions, SFHo, SFHo +  $\pi$ ,  $m_\pi = \text{Vac. mass}$ , SFHo +  $\pi$ ,  $m_\pi = 170 \text{ MeV}$  and SFHo +  $\pi$ ,  $m_\pi = 200 \text{ MeV}$ . Right: Same plots as in the left panel, but for DD2, DD2 +  $\pi$ ,  $m_\pi = \text{Vac. mass}$ , DD2 +  $\pi$ ,  $m_\pi = 170 \text{ MeV}$  and DD2 +  $\pi$ ,  $m_\pi = 200 \text{ MeV}$ .

one percent for models with the pion vacuum masses.

In general, the softening from pions leads to a higher compactness. For a given EOS with fixed effective pion mass, the softening at higher densities is inversely related to the effective mass of the pion used in that EOS. For large effective pion masses, the stellar structure is very similar to the one resulting from the EOSs without pions.

## B. Simulation details

We simulate the hydrodynamical evolution of NS mergers using a general relativistic smoothed particle hydrodynamics (SPH) code that employs the conformal flatness condition to solve the general relativistic Einstein field equations [78–82]. The initial data are constructed by imposing neutrinoless  $\beta$ -equilibrium conditions in the respective EOSs where neutrons, protons, electrons and pions (if present) are in chemical and thermal equilibrium. The stars are assumed not to have any intrinsic rotation. Our simulations begin with two NSs in a quasi-circular equilibrium orbit with an orbital separation such that the merger takes place after a few revolutions. We advect the initial electron fraction with the

fluid i.e.  $\frac{dY_e}{dt} = 0$ , which represents a rather crude treatment of weak interaction.

In this study we only consider equal mass BNS systems. We choose  $1.35\text{--}1.35M_\odot$  binaries and systems with a total mass close to the threshold binary mass for prompt black hole formation, which we estimate for the EOSs with pions from empirical relations [52]. We provide a complete list of simulations in table I for SFHo based models and table II for DD2 based models<sup>3</sup>. These include information on the total mass of the binaries, the mass of pions, the radius of cold, isolated NSs with half of the total mass of the BNS, the tidal deformability of the binary system, and the chirp mass. The tidal deformability is defined as  $\Lambda = \frac{2}{3}k_2 \left(\frac{R}{M}\right)^5$ , where  $R$  and  $M$  are the radius and the gravitational mass of the individual non-rotating NSs and  $k_2$  is the tidal Love number [83].

<sup>3</sup> In these tables we do not list all simulations performed for this study but provide only those for which we run the same total binary mass for all four versions of the EOS model. For determining the threshold binary mass for the individual EOS models we conducted additional simulations for specific total binary masses.

TABLE I. Properties of the simulated models with the SFHo EOS and the modified SFHo EOSs with pions. First column shows names of the simulated models. Second column shows the gravitational masses of BNSs,  $m_\pi$  is the effective pion mass employed in the modified EOS,  $R_{\text{ns}}$  and  $\Lambda$  are the radius and the dimensionless tidal deformability of a single NS corresponding to one of the star in the equal-mass BNS system.  $M_{\text{chirp}}$  represents the chirp mass of the BNS system. The column ‘‘Prompt collapse’’ indicates whether a BH is formed immediately after the merger or not,  $f_{\text{peak}}$  denotes the peak frequency of the GW spectrum. The  $f_{\text{peak}}$  is shown only for the models without prompt collapse.

Model	BNS masses [ $M_\odot$ ]	$m_\pi$ [MeV]	$R_{\text{ns}}$ [km]	$\Lambda$	$M_{\text{chirp}}$ [ $M_\odot$ ]	Prompt collapse	$f_{\text{peak}}$ [kHz]
SFHo_Pions_VacMass_1.35_1.35	1.35–1.35	vacuum mass	11.727	377.902	1.175	no	3.462
SFHo_Pions_170MeV_1.35_1.35	1.35–1.35	170 MeV	11.872	413.490	1.175	no	3.351
SFHo_Pions_200MeV_1.35_1.35	1.35–1.35	200 MeV	11.896	420.776	1.175	no	3.318
SFHo_Base_1.35_1.35	1.35–1.35	no pion	11.896	420.813	1.175	no	3.310
SFHo_Pions_VacMass_1.40_1.40	1.40–1.40	vacuum mass	11.700	296.937	1.219	no	3.599
SFHo_Pions_170MeV_1.40_1.40	1.40–1.40	170 MeV	11.845	324.561	1.219	no	3.530
SFHo_Pions_200MeV_1.40_1.40	1.40–1.40	200 MeV	11.874	332.950	1.219	no	3.454
SFHo_Base_1.40_1.40	1.40–1.40	no pion	11.874	332.970	1.219	no	3.419
SFHo_Pions_VacMass_1.42_1.42	1.42–1.42	vacuum mass	11.687	270.635	1.236	yes	—
SFHo_Pions_170MeV_1.42_1.42	1.42–1.42	170 MeV	11.833	296.199	1.236	no	3.621
SFHo_Pions_200MeV_1.42_1.42	1.42–1.42	200 MeV	11.864	303.134	1.236	no	3.552
SFHo_Base_1.42_1.42	1.42–1.42	no pion	11.864	303.089	1.236	no	3.499
SFHo_Pions_VacMass_1.425_1.425	1.425–1.425	vacuum mass	11.684	264.060	1.241	yes	—
SFHo_Pions_170MeV_1.425_1.425	1.425–1.425	170 MeV	11.830	289.202	1.241	yes	—
SFHo_Pions_200MeV_1.425_1.425	1.425–1.425	200 MeV	11.862	295.680	1.241	no	3.622
SFHo_Base_1.425_1.425	1.425–1.425	no pion	11.862	295.619	1.241	no	3.573
SFHo_Pions_VacMass_1.43_1.43	1.43–1.43	vacuum mass	11.681	257.484	1.245	yes	—
SFHo_Pions_170MeV_1.43_1.43	1.43–1.43	170 MeV	11.827	282.205	1.245	yes	—
SFHo_Pions_200MeV_1.43_1.43	1.43–1.43	200 MeV	11.859	288.226	1.245	yes	—
SFHo_Base_1.43_1.43	1.43–1.43	no pion	11.859	288.156	1.245	no	3.614

The chirp mass is given by  $M_{\text{chirp}} = \frac{(M_1 M_2)^{3/5}}{(M_1 + M_2)^{1/5}}$ , where  $M_1$  and  $M_2$  are BNS masses. We also indicate whether the system undergoes a prompt gravitational collapse and provide the dominant GW frequency of the postmerger phase. The dominant GW frequency is not shown for the models which experience prompt collapse.

#### IV. SIMULATION RESULTS

In this section we describe the general dynamics and the evolution of the pion contributions in our binary merger simulations. We address the postmerger GW signal and the threshold mass for prompt black-hole formation and discuss to which extent these features are affected by the presence of pions.

##### A. Dynamics and pion production in NS mergers

Apart from models undergoing a prompt gravitational collapse to a black hole, all BNS merger simulations proceed qualitatively similar, and we do not recognize any specific differences between the calculations with the base

EOSs and those with the modified EOSs with pions. Most of the simulated binaries result in the formation of a rotating NS remnant, and only a few systems with relatively large total binary masses lead to direct black hole formation after merging (to be discussed below).

In the simulations yielding a NS remnant, the merging stars form a rotating double-core structure and, while the densities in the postmerger phase increase, the remnant undergoes vivid oscillations. For the 1.35-1.35  $M_\odot$  models, the density oscillations can be seen in Fig. 9 showing the evolution of the maximum baryonic rest-mass density. The quantitative behavior is inline with existing literature results, i.e., softer EOSs lead to higher densities. This concerns the comparison between the base EOSs, SFHo and DD2, and also the comparison between the respective base EOS and the versions with pions. Smaller effective pion masses lead to softer EOSs and more compact stellar configurations and thus higher  $\rho_{\text{max}}$  in the merger remnant. Quantitatively, the maximum densities in the merger remnant are consistent with empirical relations for  $\rho_{\text{max}}$  found for a large sample of candidate EOSs without pions (see discussion below in subsection IV C).

As discussed in Sect. II, the production of pions depends on the difference between the chemical potentials

TABLE II. Properties of the simulated models with the DD2 EOS and the modified DD2 EOSs with pions. Same as Tab.I but for the models based on DD2.

Model	BNS masses [ $M_\odot$ ]	$m_\pi$ [MeV]	$R_{\text{ns}}$ [km]	$\Lambda$	$M_{\text{chirp}}$ [ $M_\odot$ ]	Prompt collapse	$f_{\text{peak}}$ [kHz]
DD2_Pions_VacMass_1.35_1.35	1.35–1.35	vacuum mass	13.048	796.159	1.175	no	2.681
DD2_Pions_170MeV_1.35_1.35	1.35–1.35	170 MeV	13.189	854.982	1.175	no	2.642
DD2_Pions_200MeV_1.35_1.35	1.35–1.35	200 MeV	13.199	871.076	1.175	no	2.597
DD2_Base_1.35_1.35	1.35–1.35	no pion	13.199	871.135	1.175	no	2.608
DD2_Pions_VacMass_1.62_1.62	1.62–1.62	vacuum mass	13.068	262.744	1.410	no	3.099
DD2_Pions_170MeV_1.62_1.62	1.62–1.62	170 MeV	13.219	287.197	1.410	no	3.030
DD2_Pions_200MeV_1.62_1.62	1.62–1.62	200 MeV	13.247	294.408	1.410	no	3.008
DD2_Base_1.62_1.62	1.62–1.62	no pion	13.247	294.465	1.410	no	2.997
DD2_Pions_VacMass_1.64_1.64	1.64–1.64	vacuum mass	13.066	243.524	1.428	yes	—
DD2_Pions_170MeV_1.64_1.64	1.64–1.64	170 MeV	13.217	266.835	1.428	no	3.137
DD2_Pions_200MeV_1.64_1.64	1.64–1.64	200 MeV	13.248	270.335	1.428	no	3.024
DD2_Base_1.64_1.64	1.64–1.64	no pion	13.248	270.407	1.428	no	3.036
DD2_Pions_VacMass_1.65_1.65	1.65–1.65	vacuum mass	13.065	234.778	1.436	yes	—
DD2_Pions_170MeV_1.65_1.65	1.65–1.65	170 MeV	13.216	256.653	1.436	yes	—
DD2_Pions_200MeV_1.65_1.65	1.65–1.65	200 MeV	13.248	260.521	1.436	no	3.127
DD2_Base_1.65_1.65	1.65–1.65	no pion	13.248	260.531	1.436	no	3.047
DD2_Pions_VacMass_1.66_1.66	1.66–1.66	vacuum mass	13.064	226.031	1.445	yes	—
DD2_Pions_170MeV_1.66_1.66	1.66–1.66	170 MeV	13.216	246.472	1.445	yes	—
DD2_Pions_200MeV_1.66_1.66	1.66–1.66	200 MeV	13.248	251.637	1.445	yes	—
DD2_Base_1.66_1.66	1.66–1.66	no pion	13.248	251.658	1.445	no	3.139

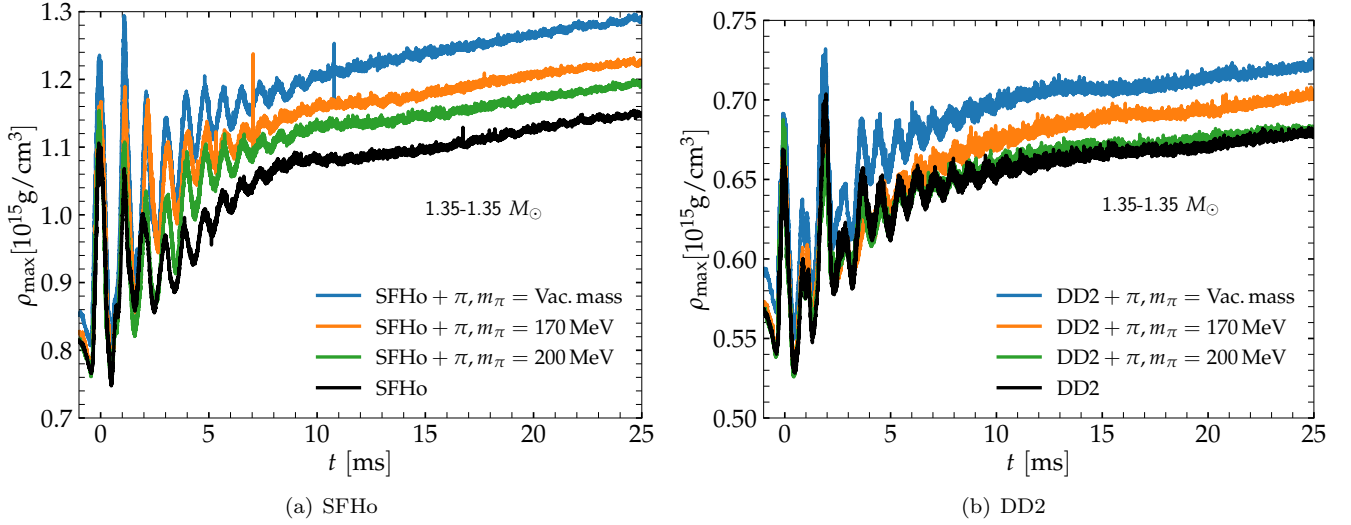


FIG. 9. Time evolution of the maximum baryonic rest-mass density for  $1.35\text{-}1.35M_\odot$  BNS systems using SFHo EOS (left panel) and DD2 EOS (right panel). The time zero corresponds to the instant of the maximum compression during the first bounce after merging (minimum in the lapse function). We evaluate the maximum baryonic rest-mass density on the SPH particle level, which is why some noise is visible.

of neutrons and protons, and through this on the density and temperature. At typical densities of NSs and NS merger remnants, the contributions from thermal pions become dominant only beyond a threshold temperature of several 10 MeV (see Figs. 2 and discussion in Sect.II).

We assess the temperature regime in the merger remnants of  $1.35\text{-}1.35M_\odot$  binary simulations in Fig. 10 visualizing the evolution of the maximum temperature and

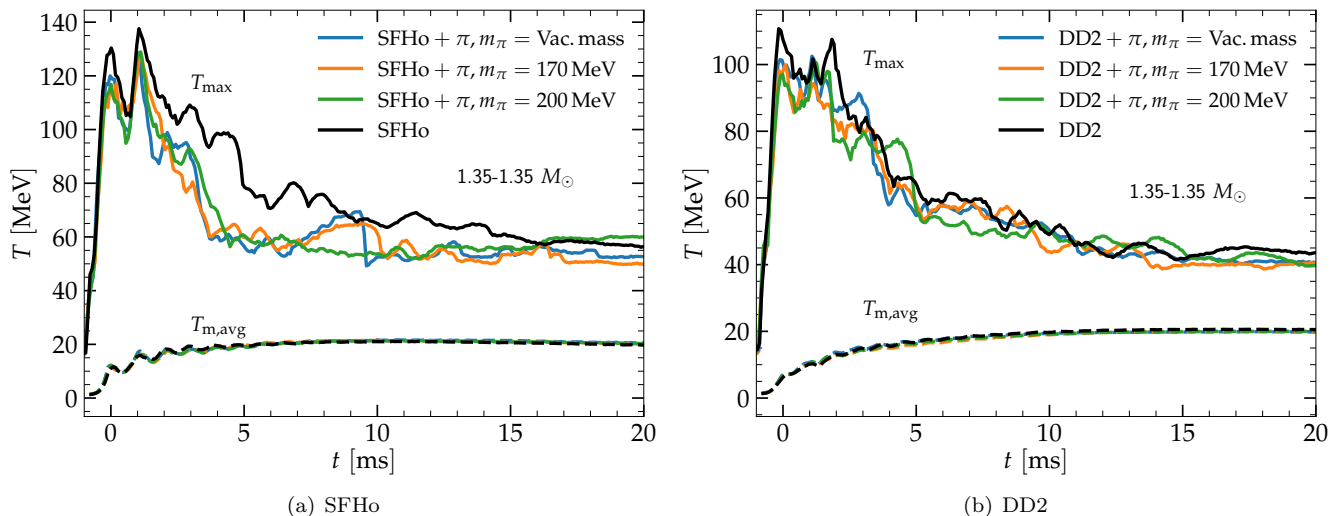


FIG. 10. Time evolution of the maximum and mass-averaged temperature for  $1.35\text{-}1.35M_{\odot}$  BNS systems using SFHo EOS (left panel) and DD2 EOS (right panel).

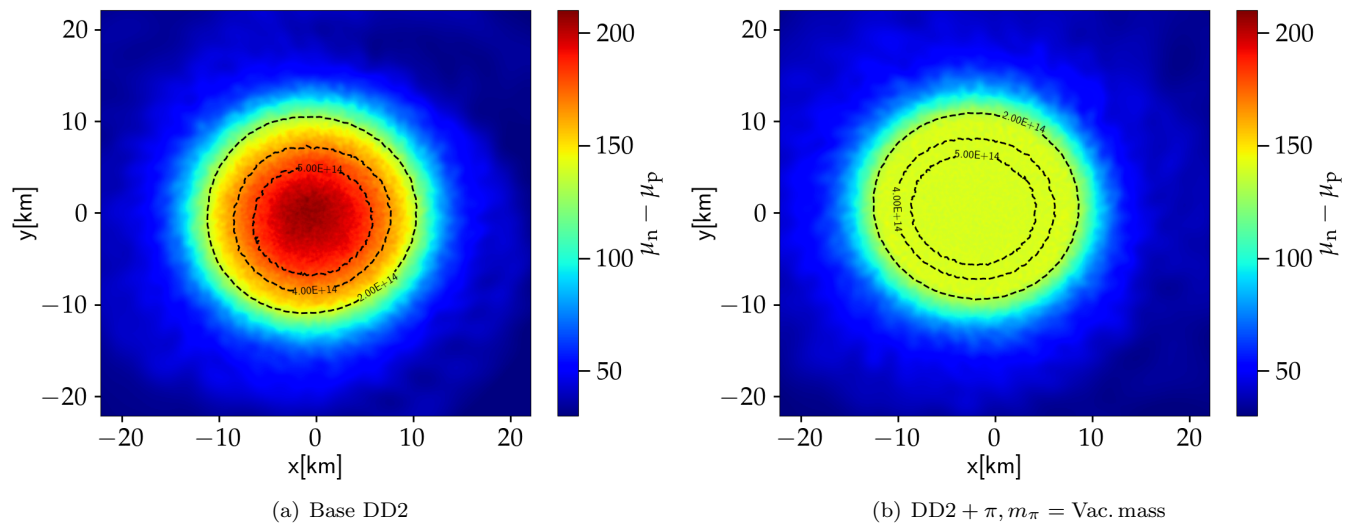


FIG. 11. The panels (a) and (b) show snapshots of neutron and proton chemical potential difference  $\mu_n - \mu_p$  in the equatorial plane for a  $1.35\text{-}1.35M_{\odot}$  BNS model after the merger, using the base DD2 EOS without pions and the modified DD2 EOS that includes pions with an effective pion masses equal to their vacuum masses, DD2 +  $\pi$ ,  $m_{\pi} = \text{Vac. mass}$ . Density regions of  $2 \times 10^{14}\text{g/cm}^3$ ,  $4 \times 10^{14}\text{g/cm}^3$  and  $5 \times 10^{14}\text{g/cm}^3$  are shown by dashed contour lines.

the mass-averaged temperature<sup>4</sup>. Although the maximum temperatures do reach about 100 MeV, such conditions are only found in a small volume in the remnant and not necessarily at the highest densities. Average temperatures in the merger remnant are significantly lower (of the order of about 20 MeV), which suggests that thermal pions likely play only a sub-dominant role in the

merger remnant of the systems considered here. Hence, we anticipate that the inclusion of pions in BNS merger simulations overall has a softening effect.

In Fig. 10(a), we observe that the models with the softer SFHo EOS lead to slightly higher maximum temperatures, which is understandable given that the stars described by this EOS collide more violently and the compression in the remnant is stronger. There is also the tendency that models with pions result in slightly lower maximum temperatures. Figure 4 clearly shows that at such high temperatures the inclusion of pions leads to a stiffening of the EOSs, which is roughly independent of

<sup>4</sup> We define a mass-averaged quantity by summing the contribution from all SPH particles weighted by the mass of the particle relative to the total mass

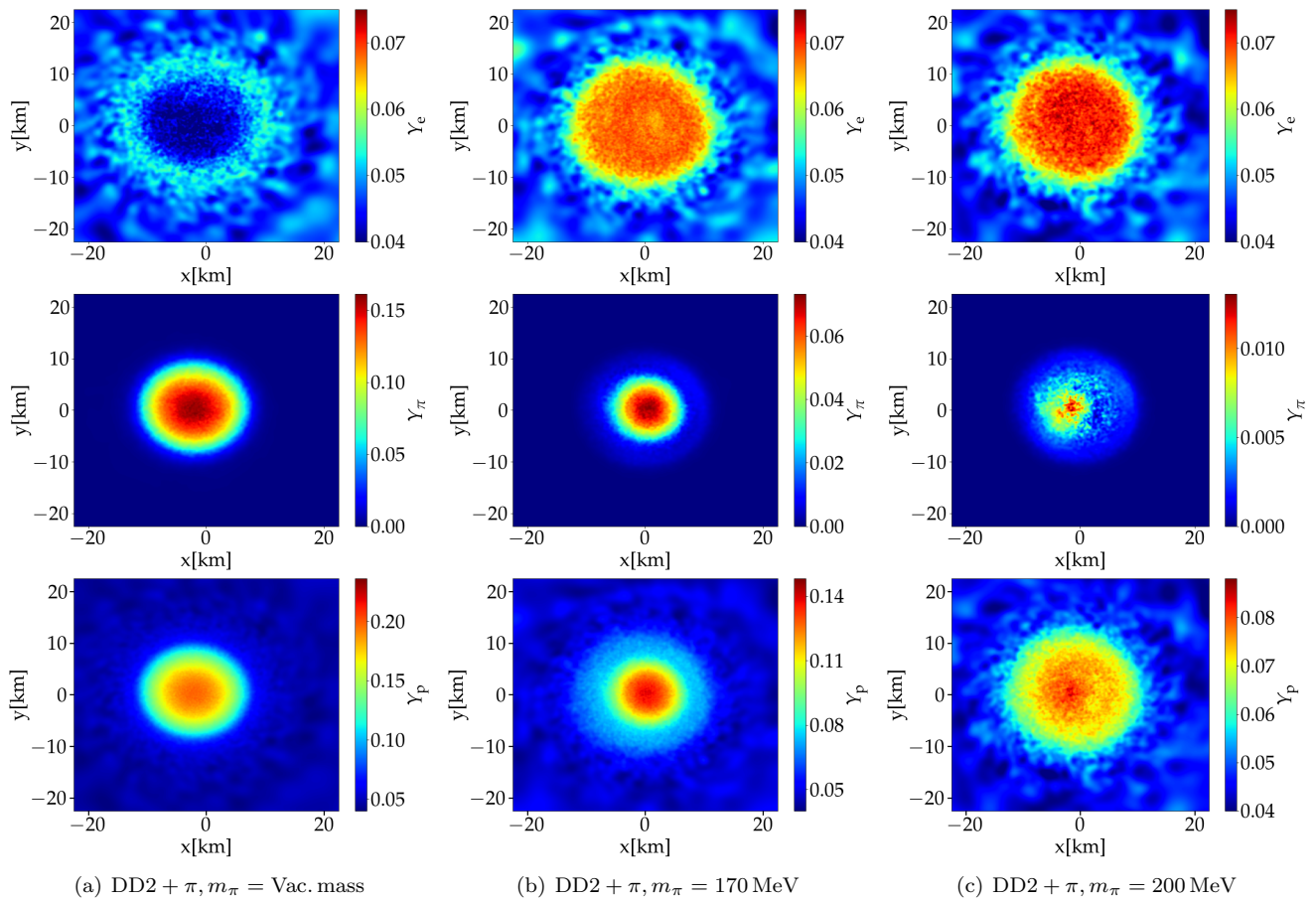


FIG. 12.  $Y_e$  distribution (top row panels),  $Y_\pi$  distribution (middle row panels) and  $Y_p$  distribution (bottom row panels) in the equatorial plane for  $1.35\text{-}1.35M_\odot$  BNS systems using DD2 +  $\pi$ ,  $m_\pi = \text{Vac. mass}$  (left column panels), DD2 +  $\pi$ ,  $m_\pi = 170 \text{ MeV}$  (middle column panels) and DD2 +  $\pi$ ,  $m_\pi = 200 \text{ MeV}$  (right column panels).

the effective pion mass. We caution that one should not overinterpret the differences in the maximum temperature between EOSs because we evaluate the temperature on the basis of individual SPH particles, which are affected by noise.

Evaluating directly the ratio between the number of thermal pions and pions in the condensate, we do indeed find that thermal pions are subdominant even in the hot merger remnant and that the main effects of pions originate from the condensate (Figs. 13 and 14 except for the case with  $m_\pi = 200 \text{ MeV}$ ).

In this respect, it is also instructive to directly compare the difference  $\hat{\mu}$  between the chemical potentials of neutrons and protons for the base model and the calculation including pions. Figure 11 shows  $\hat{\mu}$  in the equatorial plane for the DD2 base model and the model with pions adopting the vacuum pion mass. In the latter case,  $\hat{\mu}$  is limited by the pion mass ( $\sim 139.6 \text{ MeV}$  for this case), whereas  $\hat{\mu}$  reaches more than  $200 \text{ MeV}$  in the remnant's center if pions are ignored. If pions with an effective mass equal to their vacuum mass are included, a pion condensate is found throughout the whole high-density region of

the remnant. One may already conclude from the range of  $\hat{\mu}$  in the left panel of Fig. 11 that the condensation of pions in the remnant depends on the adopted effective pion mass.  $\hat{\mu}$  increases towards the center for the base model and reaches  $200 \text{ MeV}$  only in the very inner region. Hence, for  $m_\pi = 200 \text{ MeV}$ , pion condensation only takes place in the center of the remnant at the highest densities. This clearly demonstrates that the effective pion mass has a significant impact on the production of pions in BNS mergers.

These observations and their impact are further illustrated in Fig. 12, which displays snapshots of the electron fraction (upper panel), the pion fraction (middle panel) and the proton fraction (bottom panel) in the equatorial plane for a  $1.35\text{-}1.35M_\odot$  BNS merger remnant about ( $\sim 18.95$ ) milliseconds after merging, employing the pionic DD2 EOSs. The columns refer to different  $m_\pi$  increasing from left to right.

It is obvious that the inclusion of pions and their effective mass have a very strong impact on the electron fraction in the remnant, which is determined by  $\hat{\mu}$  and thus by the presence of pions and their proper-

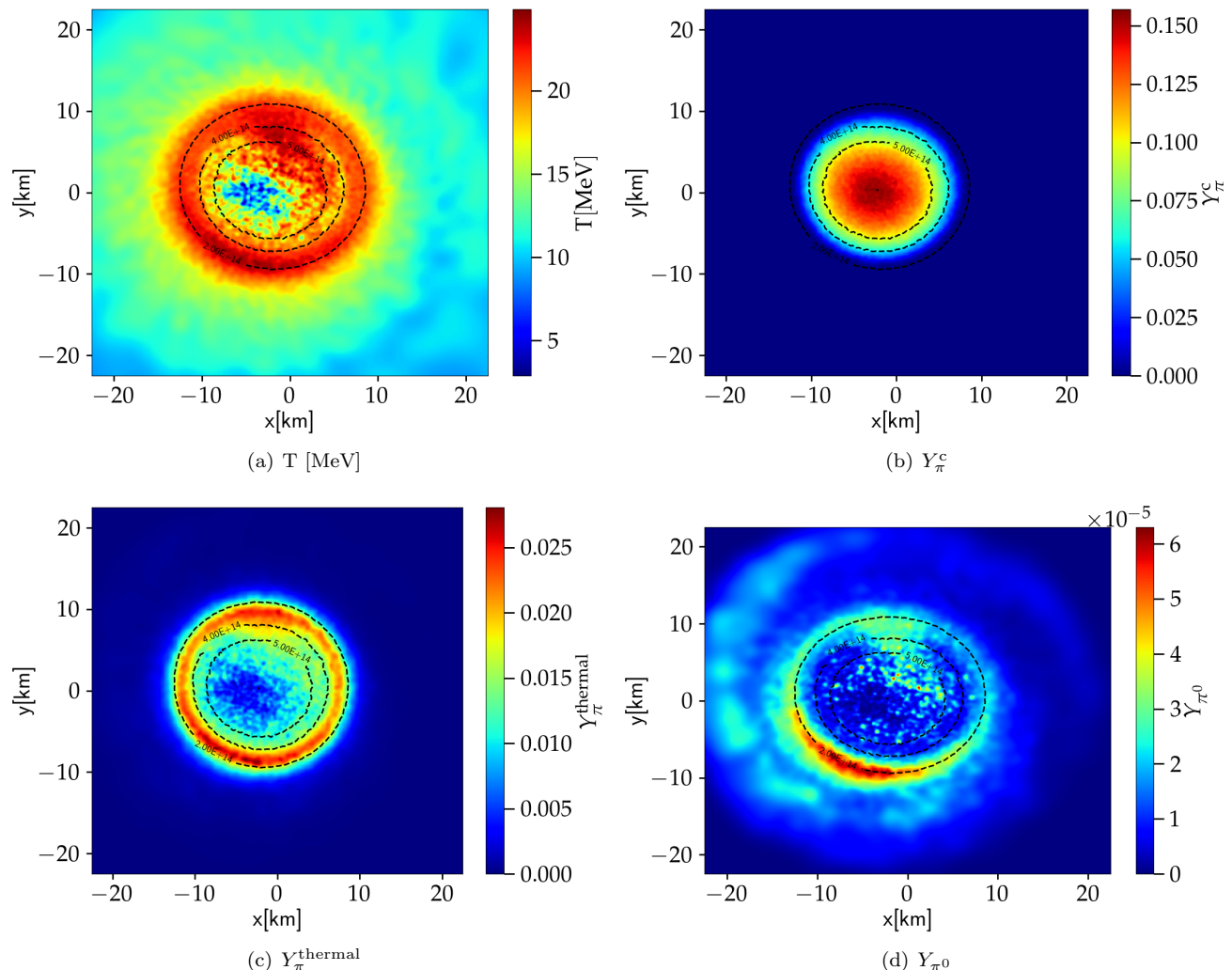


FIG. 13. Temperature,  $Y_\pi^c$ ,  $Y_\pi^{\text{thermal}}$  and  $Y_{\pi^0}$  distribution in the equatorial plane for a  $1.35\text{-}1.35M_\odot$  BNS system using the DD2 +  $\pi$ ,  $m_\pi = \text{Vac.}$  mass model. Densities of  $2 \times 10^{14}\text{g/cm}^3$ ,  $4 \times 10^{14}\text{g/cm}^3$  and  $5 \times 10^{14}\text{g/cm}^3$  are shown by dashed contour lines.

ties in the progenitor (see Fig. 7). For relatively small pion masses, the electron fraction in the remnant remains rather small while the proton fraction increases with the produced number of pions (Fig. 12(a)). For  $m_\pi = 200\text{ MeV}$  (Fig. 12(c)) the highest  $Y_e$  and the lowest  $Y_p$  is found. We recall that in these simulations we employ a rather simplistic treatment of weak interactions by ignoring neutrinos and only advecting the electron fraction. Hence, the behavior in Fig. 12 can be easily understood by the behavior in Fig. 7. For smaller effective pion masses,  $Y_e$  is strongly reduced in the initial stars, which thus yields a lower electron fraction in the remnant. The behavior of the pion fraction and the proton fraction is a consequence of the advected electron fraction. Both follow similar trends as for equilibrium NSs, i.e. a lower  $Y_e$  is accompanied by a larger proton fraction and a larger pion fraction (see Fig. 7). Despite the simple treatment of weak interactions, the panels indicate a po-

tentially significant impact by pions on the microphysics of weak interactions as they affect the conditions for the chemical potentials in the remnant.

The middle row panels in Fig. 12 visualize the pion content in the remnant depending on the effective pion mass. As expected, the volume of the region inside the HMNS where pions are present, shrinks as the effective pion mass increases. The pion content is strongly suppressed for  $m_\pi = 200\text{ MeV}$ , and only occurs in the center where  $\hat{\mu}$  reaches the pion mass. This panel illustrates that the DD2 +  $\pi$ ,  $m_\pi = 200\text{ MeV}$  model should behave very similar to the base EoS.

To address the distribution of thermal and condensed pions in different regions of the merger remnant, we show the distribution of  $Y_\pi^c$  and  $Y_\pi^{\text{thermal}}$  in Fig. 13 for the DD2 +  $\pi$ ,  $m_\pi = \text{Vac.}$  mass model along with the corresponding temperature distribution. The correlation between thermal pions and the local temperature is clear

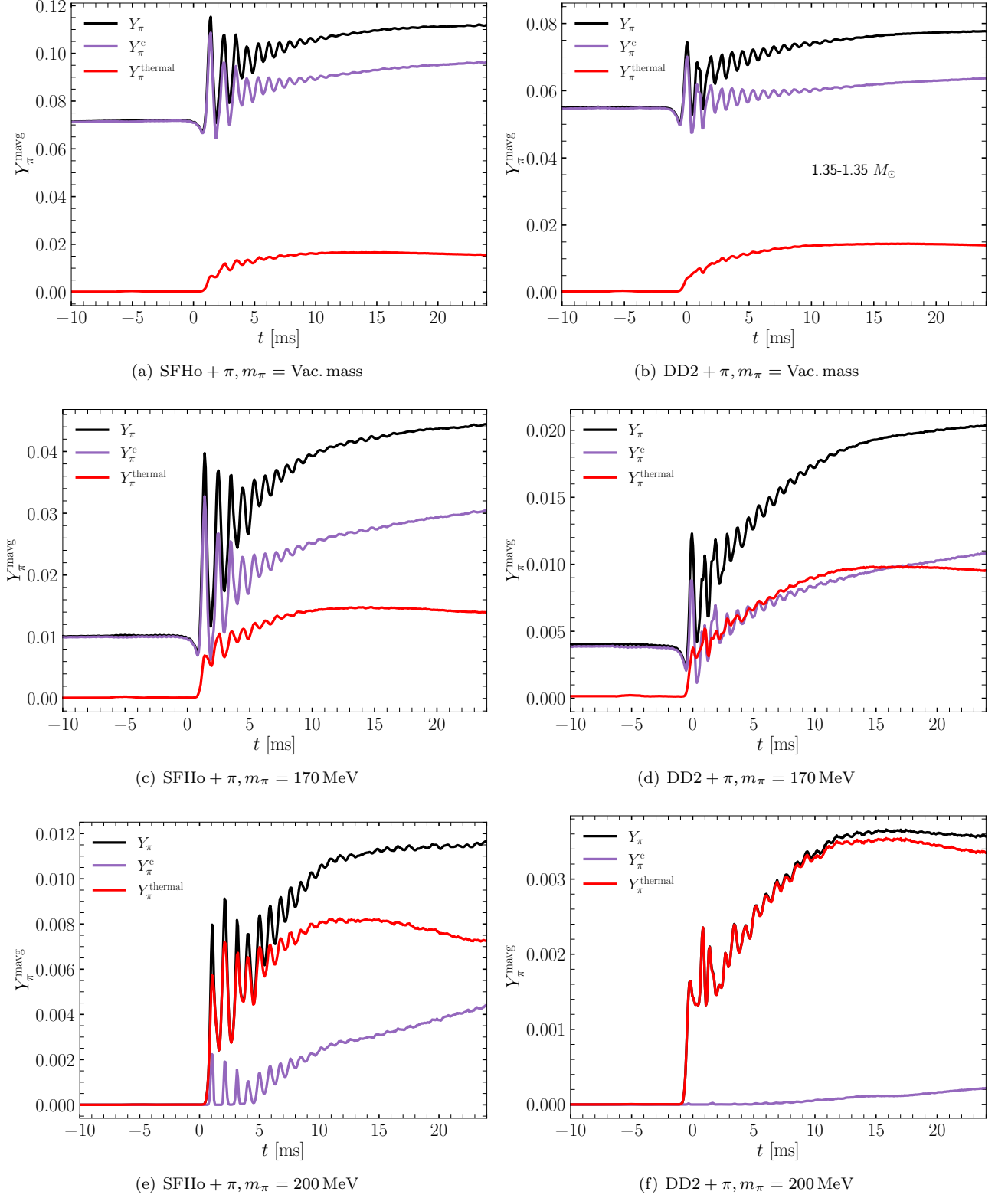


FIG. 14. Time evolution of the mass-averaged pion fraction  $Y_\pi^{\text{mavg}}$  of total pion fraction  $Y_\pi$ , condensed pion fraction  $Y_\pi^c$  and thermal pion fraction  $Y_\pi^{\text{thermal}}$  for  $1.35\text{-}1.35M_\odot$  BNS systems.

from the hot ring like structure in the merger remnant shown in Figs. 13(a) and 13(c) whereas  $Y_\pi^c$  roughly follows the density in Fig. 13(b). Although the number of neutral pions increases with temperature, the relative magnitude is very low (Fig. 13(d)). We expect the neutral pion contribution to become noticeable only at high temperatures around  $\sim 100$  MeV (particles with maximum temperature), see Fig. 1 and 3.

As temperatures and densities increase during the dynamical evolution, more pions are produced as compared to the pion content of the initial stars. We quantify the pion production in Fig. 14, which provides the mass averaged fraction of the total number of pions, condensed pions and thermal pions as function of time for both SFHo and DD2 EOSs.

One can clearly recognize that the effective pion mass sensitively affects the production of pions. For the pion mass equal to the vacuum mass, there are already a lot of pions present in the initial stars and the additional increase of the pion fraction during merging is moderate. For  $m_\pi = 170$  MeV we see a significant increase of  $Y_\pi$  by about a factor four. If the effective pion mass is as high as 200 MeV, there are no pions present during the inspiral and only the density and temperature increase after merging leads to the production of pions, which are predominantly thermal.

SFHo is softer than DD2 and thus results in higher densities in the inspiraling stars and in the postmerger remnant. Hence, the pion production is increased for the SFHo based models as compared to the EOSs relying on DD2. Considering this behavior, we anticipate that the softening of the EOS by pions is more pronounced for the softer SFHo model as compared to DD2.

## B. Gravitational wave signal

### 1. Inspiral

The GW signal reflects the dynamical evolution of BNS mergers and thus carries an imprint of the EOS. The GW inspiral signal is determined by the tidal deformability  $\Lambda$ , where we find a reduction of  $\Lambda$  of up to about 10 per cent by the inclusion of pions comparing the base models without pions and the modified EOSs with an effective pion mass equal to the vacuum mass. As anticipated from the mass-radius relations (Fig. 8), the reduction of the tidal deformability depends on the effective pion mass, and larger effective pion masses have a smaller or even negligible impact on the tidal deformability.

While these findings are not unexpected, they caution that ignoring pions in EOS calculations might potentially introduce a systematic bias if the actual effective pion mass in medium is close to its vacuum mass. This may apply to cases where microphysical parameters of the EOS as for instance the slope of the symmetry energy are inferred from the GW inspiral signal through microphysical EOS models which consider only the baryonic

and leptonic contributions. Neglecting pions and thus an additional unmodelled softening of the EOS model would lead to a systematic bias of these quantities. Clearly, whether these are severe issues, cannot be judged in our present explorative study with the rather crude incorporation of pions and especially freely chosen effective pion masses. One may expect that the actual impact of pions may become stronger for high-mass NSs and BNSs.

### 2. Postmerger

The GW signal can also contain a high-frequency component originating from the postmerger phase, i.e. the dynamical evolution of the NS remnant, whereas the high-frequency emission from a directly forming black hole in a prompt gravitational collapse is very weak. If a rotating NS merger remnant forms, one may expect a pronounced impact of pions because the postmerger remnant features finite temperatures and higher densities than the inspiralling NSs. The GW emission of a NS postmerger remnant is dominated by a single, roughly constant frequency,  $f_{\text{peak}}$ , which reflects the main oscillation mode of the central object and occurs as a strong peak in the GW spectrum.

Figure 15 shows the amplitude of the postmerger GW spectra for an observer at 20 Mpc along the polar axis for 1.35-1.35 $M_\odot$  BNS systems with the SFHo EOSs (left panel) and DD2 EOSs (right panel). It is known that the main frequency scales tightly with NS radii as a measure for the softness of the EOS [38]. The DD2 models oscillate at significantly lower frequencies of about 2.6 kHz compared to more than 3 kHz for the SFHo based EOSs.

Considering the impact of pions, we find that their inclusion shifts the main peak to higher frequencies. This effect is more pronounced for smaller effective pion masses, which is not surprising considering for instance the mass-radius relations of these EOSs. The shift appears to be slightly more pronounced for the SFHo based models with a modification of about 200 Hz. For  $m_\pi = 200$  MeV, the main peak is hardly affected by the inclusion of pions, which is consistent with the findings in Sect. IV A, namely that there is only a small contribution by pions for this model. We also recognize an impact on the secondary features of the GW spectrum, i.e. subdominant frequency peaks that have for instance been associated with the formation of massive tidal bulges at the surface of the remnant or a non-linear coupling of the dominant mode and the quasi-radial oscillation of the central object (see [5] for a detailed discussion). Interestingly, it seems that at least for the SFHo based models the influence of pions on those features is stronger.

We display the frequency shift of the main peak and the quantitative impact of the chosen effective pion mass in Fig. 16, which reveals a clear dependence on  $m_\pi$ . The shifts also indicate (based on only these two base EOSs) that there may be a stronger impact for softer EOSs. This may not be surprising since such models

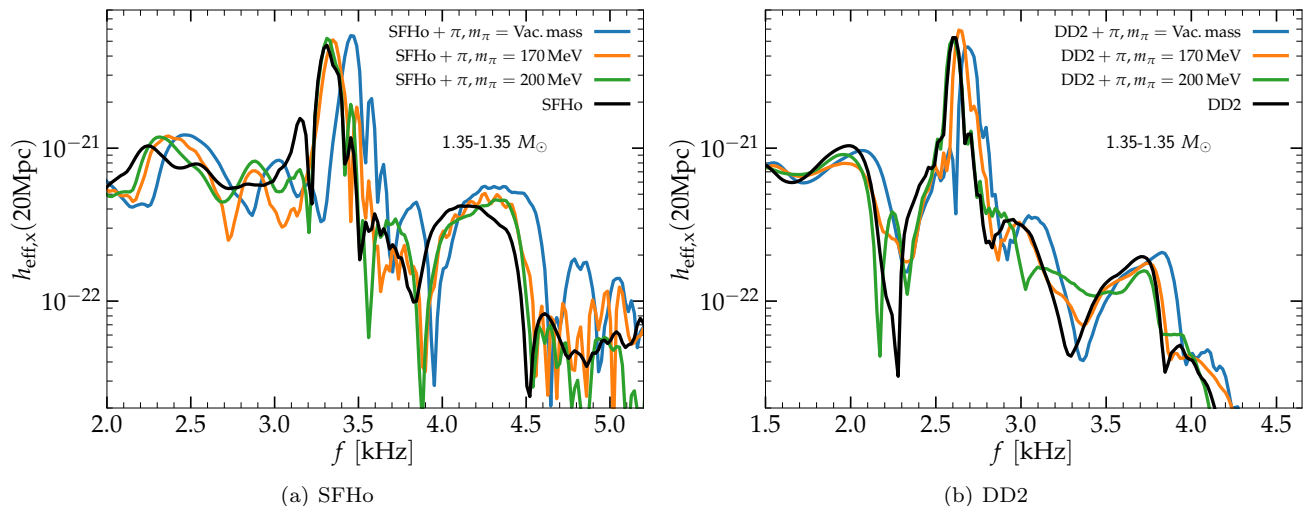


FIG. 15. Comparison of the the cross-polarization amplitude of the GW spectra for an observer at 20 Mpc along the polar axis with the SFHo and DD2 EOSs for  $1.35\text{-}1.35 M_{\odot}$  binaries. The color scheme is the same as in Figs. 9 and 10.

reach higher densities and temperatures, where pions may lead to a strong impact. We observe similar trends for the frequency shift also for other binary masses (see Tabs. I and II).

### C. Empirical relations for postmerger GW frequencies

By surveying a large sample of EOS models without pions, a number of empirical relations have been identified, which relate the main postmerger frequency to stellar properties of isolated, cold, nonrotating NSs such as their radii or tidal deformability, e.g. [37, 38, 40, 42–45, 47, 48, 50, 51]. These relations are important because they are the basis for inferring these stellar parameters from a measurement of  $f_{\text{peak}}$ , e.g. [84].

Our results so far showed that the inclusion of pions affects both the stellar parameters of isolated NSs and the properties of the postmerger GW emission. As the empirical relations are built on models ignoring pions, it is thus important to investigate whether models with pions do follow these empirical relations or whether there are deviations. This is relevant because the use of the existing relations could introduce a bias when they are employed for EOS constraints.

We also recall that the impact of pions may be different in different regimes. The analysis in Sect. II shows that including pions can lead to a softening of the EOS compared to a base model without pions or to a stiffening for instance at high temperatures. Hence, the effect of pions is not straightforward to estimate.

We address this aspect by evaluating mass-dependent empirical relations, i.e. relations for a fixed total binary mass, since those yield the tightest relations and possible deviations can be identified more easily. Specifically, we

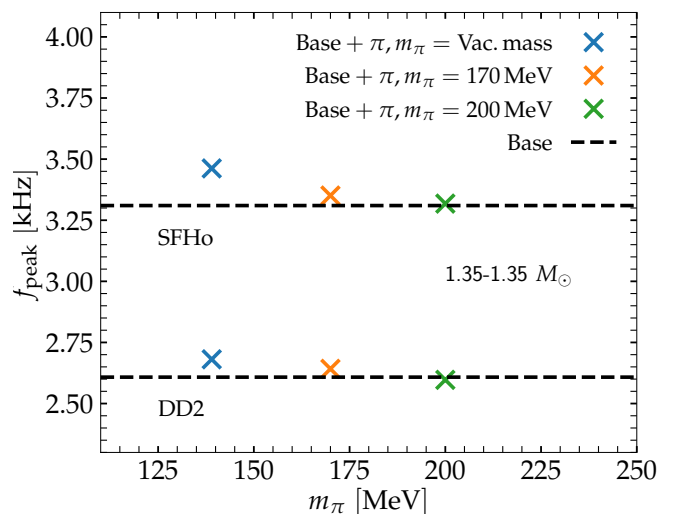


FIG. 16. The dominant postmerger GW oscillation frequency with respect to the pion mass employed in the modified EOSs for  $1.35\text{-}1.35 M_{\odot}$  simulations.  $f_{\text{peak}}$  for the respective base EOS is indicated by the black dashed line.

check the results for  $1.35\text{-}1.35 M_{\odot}$  binaries.

Figure 17 displays the relation between  $f_{\text{peak}}$  and the radius  $R_{1.6}$  of nonrotating NSs with a mass of  $1.6 M_{\odot}$  [38]. The plot includes results from our new calculations and older data from [50] for a larger set of EOSs none of which considers pions. The solid black line is a least square polynomial fit to the data from [50], i.e. it describes the behavior of EOS models without pions. The band illustrates the maximum scatter in this relation; we choose the width to equal the maximum residual between fit and data.

The figure shows that the inclusion of pions does not

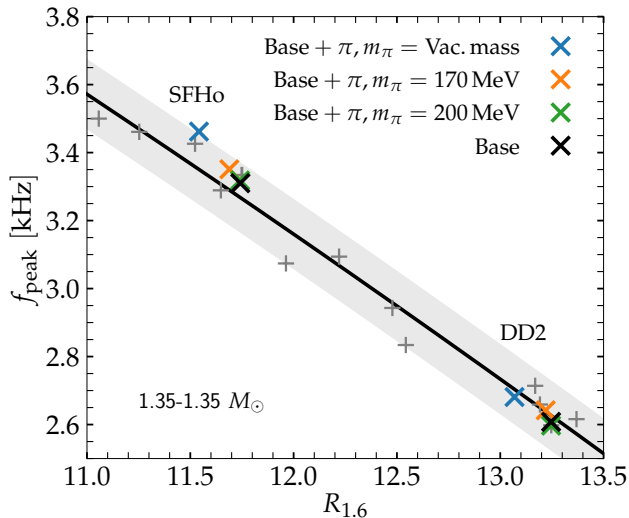


FIG. 17. Dominant postmerger GW frequency,  $f_{\text{peak}}$  versus the radius of non-rotating  $1.6M_{\odot}$  NS for  $1.35\text{-}1.35M_{\odot}$  BNS models using the modified SFHo and DD2 EOSs (crosses) compared to models using different microphysical EOSs which do not include pions (plus signs). The solid curve is a least square fit to the data points of EOSs without pions, with the gray shaded area visualizing the largest deviation of the data from the least squares fit.

lead to strong deviations from the empirical  $f_{\text{peak}}\text{-}R_{1.6}$  relation. The presence of pions simultaneously changes the properties of the postmerger GW emission and the parameters of nonrotating NSs. The modifications by pions to a large extent cancel each other. Only for the SFHo model with  $m_{\pi}$  equal to the mass in vacuum,  $f_{\text{peak}}$  is shifted to higher frequencies such that it is marginally compatible with the band defining the inherent scatter of this relation (see also [85] for an extensive discussion of frequency deviations in empirical relations for the postmerger GW signal). These findings indicate that at most there could be a slight bias for very soft EOS models in the sense that the actual relation lies at slightly higher frequencies if the actual effective pion mass is close to its vacuum value.

A similar picture arises for relations which link the dominant postmerger frequency and the tidal deformability [42, 43, 50]. This is demonstrated in Fig. 18. Again, models with pions are in agreement with relations that are based on models without pions. SFHo +  $\pi$ ,  $m_{\pi} = \text{Vac. mass}$  model leads to a somewhat more pronounced frequency shift, and this case is only marginally compatible with the old relation.

We furthermore investigate a relation that connects the dominant postmerger frequency and the maximum rest-mass density,  $\rho_{\text{max}}^{\text{max}}$ , which occurs during the early evolution in the postmerger remnant, i.e. the highest maximum rest-mass density that occurs during the first five milliseconds after merging [50, 86]. This correlation is useful because one can estimate the density regime of the central object. Figure 19 reveals that models with pi-

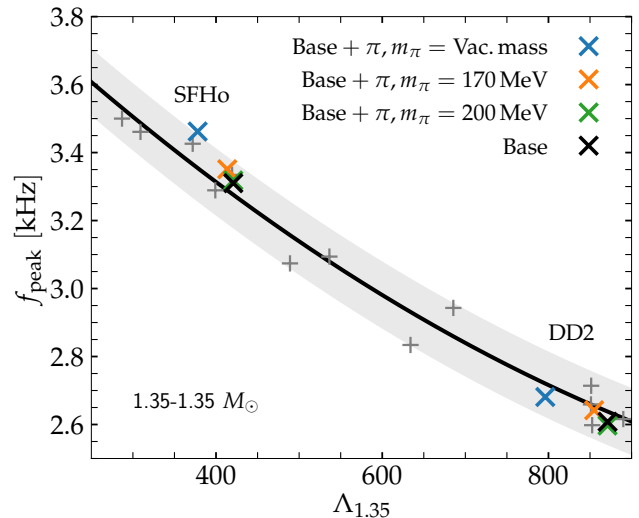


FIG. 18. Dominant postmerger GW frequency,  $f_{\text{peak}}$ , versus the tidal deformability  $\Lambda$  of  $1.35\text{-}1.35M_{\odot}$  BNSs using modified SFHo and DD2 EOSs (crosses) compared to models using different microphysical EOSs which do not include pions (plus signs). The solid curve is a least square fit to the data points of EOSs without pions, with the gray shaded area visualizing the largest deviation of the data from the least squares fit.

ons also follow this relation with good accuracy and that there do not occur any particularly strong deviations. Compared to the base model, the calculation adopting a pion mass equal to the vacuum mass exhibits a slight increase in  $\rho_{\text{max}}^{\text{max}}$ . This is consistent with the behavior in Fig. 9(a) and 9(b), which also indicate an increased softening of the EOS by the inclusion of pions with this effective mass. This specific model features the largest pion content (mostly condensate pions, see Fig. 14) and leads to the most significant shifts in Fig. 17, 18 and 19, not only parallel to the black solid lines but also perpendicular to it. One may hence not fully exclude that more extreme models with even higher pion content could lead to somewhat stronger deviations from the various empirical relations. However, given that our models provide a decent coverage of the allowed parameter space, substantially stronger deviations seem unlikely.

#### D. Threshold mass

The high-density EOS determines the outcome of BNS mergers, i.e. the nature, evolution and stability of merger remnants, which can be either a black hole for high total binary masses or a massive, rotating NS if the total mass of the system does not exceed the threshold mass for a prompt gravitational collapse. It is thus important to understand whether pions do have an influence in this context as well.

Specifically, we consider the threshold binary mass  $M_{\text{thres}}$  for prompt black-hole formation, which can also be regarded as a general measure for the stability of

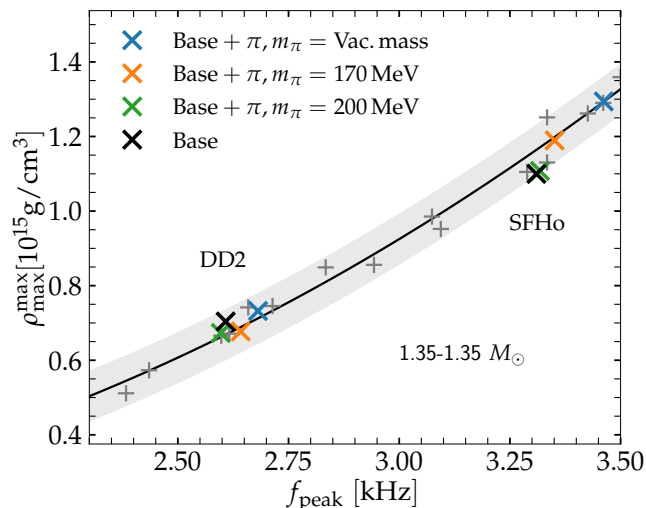


FIG. 19. Maximum rest-mass density  $\rho_{\max}^{\max}$  of the early post-merger evolution as a function of the dominant postmerger GW frequency,  $f_{\text{peak}}$ , for a  $1.35\text{-}1.35M_{\odot}$  BNSs using modified SFHo and DD2 EOSs (crosses) compared to models using different microphysical EOSs which do not include pions (plus signs). The solid curve is a least square fit to the data points of EOSs without pions, with the gray shaded area visualizing the largest deviation of the data from the least squares fit.

the remnant. As in previous work [39, 52, 87] we determine  $M_{\text{thres}}$  by considering simulations with different total binary masses  $M_{\text{tot}}$  for a given EOS model. Within this set of calculations we identify the model with the highest  $M_{\text{tot}} = M_{\text{stab}}$  that does not undergo a direct collapse, and the lightest system with  $M_{\text{tot}} = M_{\text{unstab}}$  which directly forms a black hole. The threshold mass is then defined by  $M_{\text{thres}} = 0.5(M_{\text{stab}} + M_{\text{unstab}})$ . We consider the evolution of the minimum lapse function  $\alpha_{\min}$  to distinguish prompt black-hole formation from a delayed gravitational collapse. If  $\alpha_{\min}$  continuously decreases after the first contact, a prompt collapse occurs. If  $\alpha_{\min}$  levels off and increases, this indicates a bounce of the merger remnant and we classify this behavior as a delayed collapse. This procedure and the definition of  $M_{\text{thres}}$  imply that  $M_{\text{thres}}$  can only be determined with a finite accuracy apart from other numerical errors in the simulations. For every EOS model in this study we compute the threshold mass to at least within  $\pm 0.02 M_{\odot}$ , i.e.  $M_{\text{unstab}} - M_{\text{stab}} = 0.04 M_{\odot}$ .

Table III lists the threshold mass for all EOS models<sup>5</sup>. For both base EOS models we find that  $M_{\text{thres}}$  is systematically reduced by the inclusion of pions. For a given

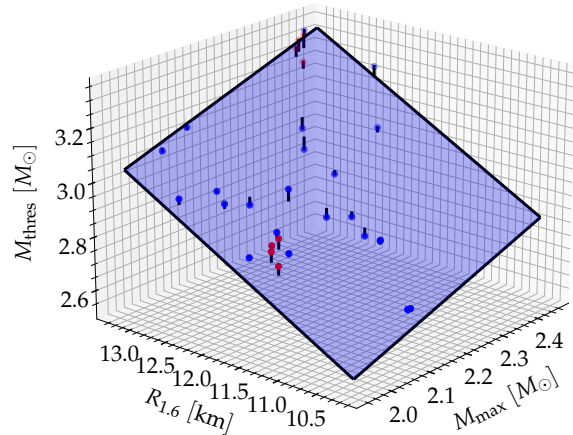


FIG. 20. Threshold binary mass for prompt collapse as a function of the radius  $R_{1.6}$  of a  $1.6 M_{\odot}$  NS and the maximum mass  $M_{\text{max}}$  of nonrotating NSs. Blue dots display results for EOS models without pions, and the blue plane shows a least square fit to these data (set “b” from [52]). Vertical lines visualize the deviation between the respective data point and the fit (plane). Red dots show the data for the simulations with the EOSs employed in this study.

base model the decrease of  $M_{\text{thres}}$  is stronger for smaller  $m_{\pi}$  and can be as large as  $0.08 M_{\odot}$  (about two per cent of  $M_{\text{thres}}$ ). This is in line with the behavior already found in the analysis of the GW emission, where smaller effective pion masses lead to a generally more pronounced softening of the EOS. Still, this behavior may not be obvious, since the inclusion of pions actually leads to a stiffening of the EOS in the regime of very high temperatures, which is not strongly depending on the pion mass. Apparently, the overall softening has a stronger impact on the stability, which may be explained by the fact that only a very small volume of the remnant features conditions where a stiffening by pions could occur.

As features of the GW signal, the threshold mass for prompt black-hole formation follows empirical relations, which describe  $M_{\text{thres}}$  as function of stellar parameters of cold, nonrotating NSs. A number of such relations have been put forward based on the consideration of a large set of different EOS models without pions [39, 41, 46, 49, 52–55, 87]. These relations typically depend on two stellar parameters including the maximum mass  $M_{\text{max}}$  of nonrotating NSs. A bi-linear ansatz

$$M_{\text{thres}}^{\text{fit}}(M_{\text{max}}, Y) = aM_{\text{max}} + bY + c \quad (1)$$

works well with fit parameters  $a$ ,  $b$  and  $c$  and  $Y$  being either the radius  $R_{1.6}$  of a  $1.6M_{\odot}$  NS or radius  $R_{\text{max}}$  of a non-rotating neutron star at its maximum mass or tidal deformability  $\Lambda_{1.4}$  of a  $1.4M_{\odot}$  NS or tidal deformability  $\tilde{\Lambda}_{\text{thres}}$  at the threshold mass [52, 87]. All these stellar parameters are listed in Tab. III.

<sup>5</sup> The values for  $M_{\text{thres}}$  for our base models slightly deviate from the ones given in [52] for the same EOS. The reason is that  $M_{\text{thres}}$  is determined by a bracketing method considering the outcome of binary simulations with different total masses, and in this study we obtain  $M_{\text{thres}}$  with higher accuracy to within  $\pm 0.02 M_{\odot}$ . We note that the outcome of the respective simulation data are fully consistent with each other.

TABLE III. Determination of threshold mass. First column gives the different EOSs models used in this paper.  $M_{\text{thres}}$  is the threshold binary mass for prompt collapse.  $M_{\text{max}}$  is the maximum mass of the non-rotating NS,  $R_{1.6}$  is the radius of a  $1.6 M_{\odot}$  nonrotating NS,  $R_{\text{max}}$  is the radius of the nonrotating maximum mass NS.  $\Lambda_{1.4}$  and  $\tilde{\Lambda}_{\text{thres}}$  are the tidal deformability of a  $1.4 M_{\odot}$  NS and the tidal deformability of a binary system with a total mass equal to  $M_{\text{thres}}$ . The last four columns provide an estimated  $M_{\text{thres}}^{\text{fit}}$  using available fit formulae [52] of the form  $M_{\text{thres}}^{\text{fit}} = M_{\text{thres}}^{\text{fit}}(M_{\text{max}}, Y)$  with  $Y$  being either  $R_{1.6}$ ,  $R_{\text{max}}$ ,  $\Lambda_{1.4}$  or  $\Lambda_{\text{thres}}$ . For the estimate we employ the respective values of  $M_{\text{max}}$  and  $Y$  for the EOS model of the given row. The fit formulae are obtained from models without pions and thus the estimates allow to assess the performance of these relations for models including pions. The difference,  $M_{\text{thres}} - M_{\text{thres}}^{\text{fit}}(M_{\text{max}}, Y)$ , between the actual threshold mass (second column) and the estimate by the respective fit formula is given in parentheses. We quote the maximum residuals of the respective fits in parentheses in the third line (see [52]).

Model	$M_{\text{thres}}$	$M_{\text{max}}$	$R_{1.6}$	$R_{\text{max}}$	$\Lambda_{1.4}$	$\tilde{\Lambda}_{\text{thres}}$	$M_{\text{thres}}^{\text{fit}}$ ( $Y = R_{1.6}$ )	$M_{\text{thres}}^{\text{fit}}$ ( $Y = R_{\text{max}}$ )	$M_{\text{thres}}^{\text{fit}}$ ( $Y = \Lambda_{1.4}$ )	$M_{\text{thres}}^{\text{fit}}$ ( $Y = \tilde{\Lambda}_{\text{thres}}$ )
(Max. dev./ $M_{\odot}$ )							(0.042)	(0.059)	(0.056)	(0.085)
	[ $M_{\odot}$ ]	[ $M_{\odot}$ ]	[km]	[km]			[ $M_{\odot}$ ]	[ $M_{\odot}$ ]	[ $M_{\odot}$ ]	[ $M_{\odot}$ ]
SFHo + $\pi$ , Vac. mass	2.810	2.017	11.542	10.085	296.937	290.362	2.806(0.004)	2.804(0.006)	2.784(0.026)	2.796(0.014)
SFHo + $\pi$ , 170 MeV	2.845	2.026	11.688	10.212	324.561	292.701	2.835(0.010)	2.832(0.013)	2.811(0.034)	2.816(0.029)
SFHo + $\pi$ , 200 MeV	2.855	2.038	11.741	10.277	332.950	291.953	2.851(0.004)	2.850(0.005)	2.825(0.030)	2.832(0.023)
SFHo Base	2.870	2.056	11.743	10.285	332.970	282.036	2.861(0.009)	2.859(0.011)	2.835(0.035)	2.830(0.040)
DD2 + $\pi$ , Vac. mass	3.250	2.381	13.069	11.692	639.278	256.841	3.257(-0.007)	3.271(-0.021)	3.271(-0.021)	3.228(0.022)
DD2 + $\pi$ , 170 MeV	3.290	2.390	13.220	11.791	699.649	261.744	3.287(0.003)	3.294(-0.004)	3.325(-0.035)	3.256(0.034)
DD2 + $\pi$ , 200 MeV	3.310	2.403	13.246	11.865	700.166	256.079	3.298(0.012)	3.314(-0.004)	3.333(-0.023)	3.259(0.051)
DD2 Base	3.322	2.417	13.246	11.899	700.146	250.548	3.306(0.016)	3.327(-0.005)	3.341(-0.019)	3.263(0.059)

The inclusion of pions in an EOS model changes simultaneously the stellar parameters of cold, nonrotating NSs and the threshold mass for black-hole formation. It is thus important to check if the models with pions do follow these relations which are obtained by fits to EOS models without pions. We note that these relations are for instance employed to establish constraints on NS properties and are generally used to interpret BNS merger observations. Table III provides the estimated threshold mass for all models of this study using empirical relations constructed based on EOSs without pions [52], where we insert the stellar parameters of our modified and the original EOS tables. Specifically, we list estimates based on the fits numbered 1, 15, 29 and 43 in [52], which employ the EOS set labeled “b” therein that contains viable EOS models without phase transition to deconfined quark matter. The EOS models with pions follow these relations with very good accuracy and one cannot identify significant deviations. The differences between the fits and the actual threshold mass are provided in Tab. III. The deviations are generally small, especially in comparison to the maximum residuals of the fits (see Tab. III).

The performance of the fits is also visualized in Fig. 20, which shows  $M_{\text{thres}}^{\text{fit}}(M_{\text{max}}, R_{1.6})$ . The models with pions (red data points) do not feature any considerable deviations. A similar behavior is found for other empirical relations of [52].

Generally, this comparison shows that such type of empirical relations for  $M_{\text{thres}}^{\text{fit}}$  are accurate and can be used although they neglect pions. This is because pions impact the threshold mass and stellar parameters of NSs

such that the resulting effects nearly cancel each other. This also implies that EOS constraints based on relations for the threshold mass as in [52, 88, 89], are not affected by ignoring pions.

## E. Mass ejection

We finally address the mass ejection of BNS mergers, which is relevant for the nucleosynthesis of heavy elements through the rapid neutron-capture process and electromagnetic counterparts, so-called kilonovae, e.g. [1–7, 9, 11, 12]. Clearly, a key quantity is the ejecta mass  $M_{\text{ej}}$ , which determines the overall production of heavy elements and the properties of the electromagnetic transient. Mass ejection of BNS mergers includes several phases and with the simulations described here we can only assess the dynamical ejecta, i.e. the material which becomes gravitationally unbound during the first few 10 milliseconds after merging.

Figure 21 shows the amount of unbound material as function of time for the EOS models based on SFHo (left panel) and DD2 (right panel) considering  $1.35$ - $1.35 M_{\odot}$  binaries. We clearly recognize that dynamical mass ejection is enhanced for models with pions and that smaller effective pion masses tend to produce more unbound matter. This behavior may be expected since softer EOSs yielding smaller NS radii lead to larger ejecta masses based on studies which ignore pions [90, 91]. However, the softening by the inclusion of pions is relatively minor and NS radii do not change by a lot in particular for larger effective pion masses. In this sense the impact of

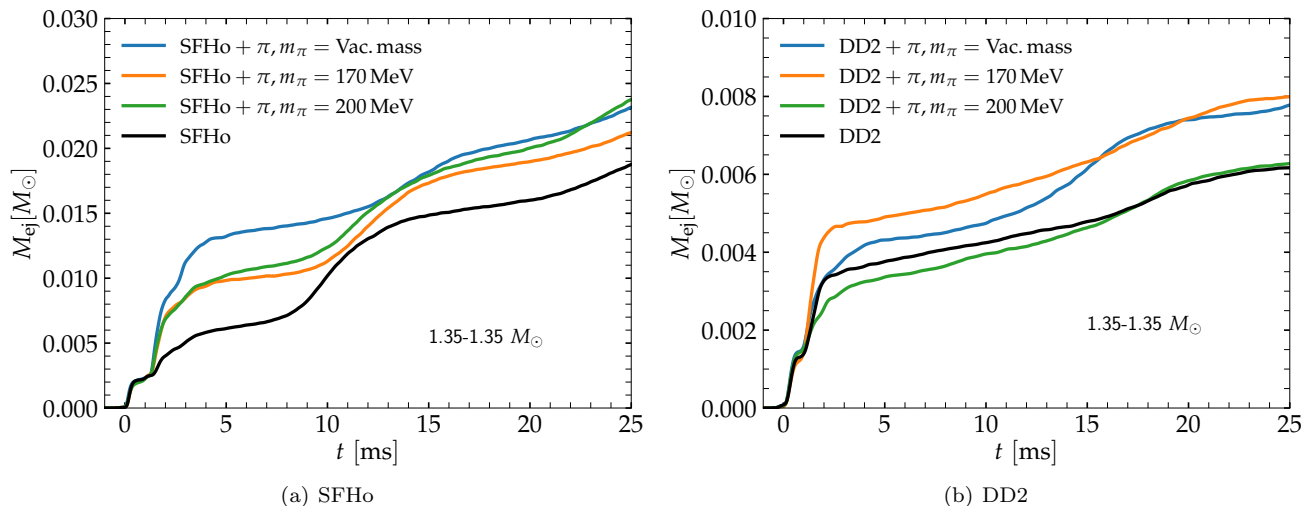


FIG. 21. Time evolution of the ejecta mass for 1.35-1.35  $M_{\odot}$  BNS mergers using modified SFHo EOSs and DD2 EOSs along with their base EOSs. Time zero corresponds to the instant when the minimum lapse function features a first minimum.

pions visible in Fig. 21 is stronger than expected. Based on previous work one would expect  $M_{\text{ej}}$  to increase by only a few percent if NS radii decrease by one or two percent, employing fit formulae that link the ejecta mass and NS radii (see e.g. Fig.22 in [12] based on fits from [92–95]). In Fig. 21 we find an increase of more than 20% in the dynamical ejecta mass for models employ effective pion masses equal to the vacuum values.

The absolute values of the base models in Fig. 21 at about 10 ms after merging are compatible with the results in [90], where  $M_{\text{ej}}$  is determined at the same time. Also, typical estimates from the existing fit formulae are roughly compatible with  $M_{\text{ej}}$  at about 10 ms after the collision.

We remark that relations between  $M_{\text{ej}}$  and NS parameters generally show a large scatter and that the ejecta mass is very sensitive to numerics and is certainly not fully converged in the simulations in addition to missing physics in the calculations (see e.g. discussion in [12]). This may also explain why there is no exact hierarchy with respect to  $m_{\pi}$ . The differences in Fig. 21 are hence only tentative but caution that ignoring pions might have a more pronounced impact on the mass ejection than suggested by the change of stellar properties of cold, nonrotating NSs. This might in particular affect attempts to infer EOS constraints from observed kilonovae (e.g. [93]). We note that the inclusion of pions does affect the EOS in a complicated non-continuous way in different regimes including softening and stiffening with respect to a base model. This may as well contribute to the behavior seen in Fig. 21.

We note that at most a very small fraction of the ejecta ( $\sim 1\%$  for SFHo, 0% for DD2) originates from densities beyond the threshold density where pion condensation sets in at about  $3 \times 10^{14}$  g/cm<sup>3</sup> in beta-equilibrium (see Fig. 7). Hence, in merger models with pions the initial

proton fraction of the ejecta remains basically unaffected compared to the base model. This may suggest that the impact of pions on the composition of the ejecta is only a secondary effect even if weak interactions were taken into account in the simulations.

Figure 22 shows the evolution of the torus mass as function of time, where we define the torus as material with a density below  $10^{13}$  g/cm<sup>3</sup> as a coarse estimate. This quantity can serve as a rough estimate of the amount of secular ejecta, which consists of a fraction of a few ten per cent of this torus material (see, e.g., [96] for an extensive analysis of torus ejecta). Tentatively, we again observe an increase of the torus mass for models which include pions (except for the DD2 based EOS with  $m_{\pi} = 200$  MeV). Considering the change of TOV properties by the inclusion of pions, one would expect a decrease of the torus mass considering fit formulae for the torus mass in the literature (see Fig. 23 in [12] compiling fits from [94, 95, 97]).

## V. CONCLUSIONS

We study the impact of pions on BNS mergers by considering neutral and charged pions as a free non-interacting boson gas, which we add to an existing base EOS. We use the temperature and composition dependent SFHo and DD2 EOSs [62–66]. Although the pion mass may change in a dense medium [58, 59, 61, 68], for this study we assume a constant value of an effective pion mass under all thermodynamical conditions. To assess the impact of changes in the pion mass, we choose different values for a constant effective pion mass. We consider calculations adopting the vacuum values of the pion masses, 170 MeV and 200 MeV.

Pions in dense matter can occur as a condensate, which

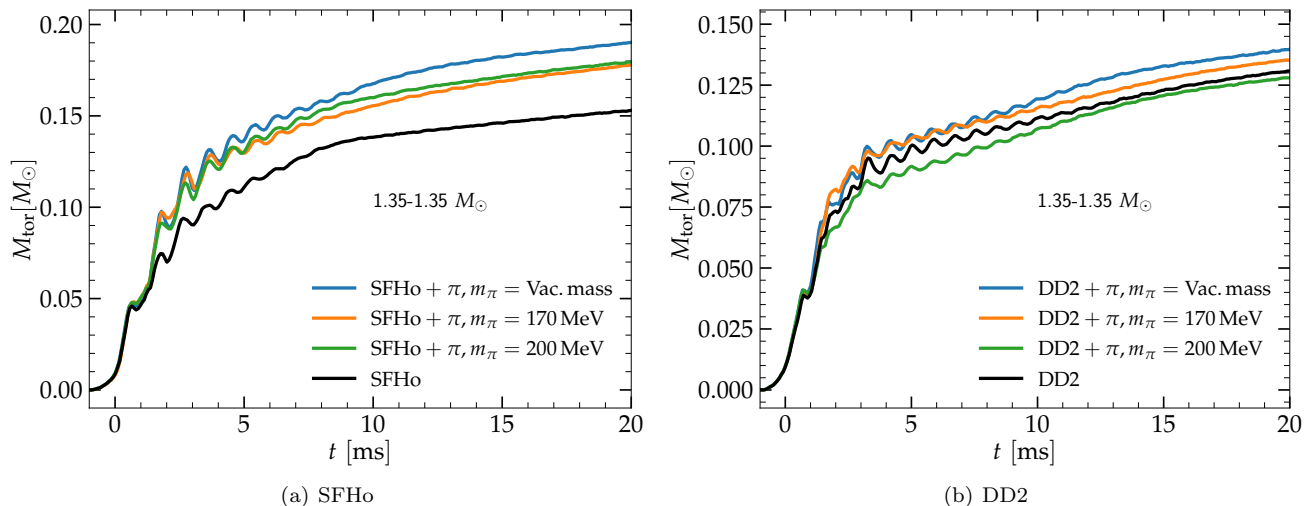


FIG. 22. Time evolution of the torus mass for  $1.35\text{-}1.35M_{\odot}$  BNS mergers using modified SFHo EOSs and DD2 EOSs along with their base EOSs. Time zero corresponds to the instant when the minimum lapse function features a first minimum.

does not directly add to the pressure, but affects the total pressure at a given  $Y_e$  by changing the equilibrium conditions and thus the baryonic contribution. This leads to a softening of the NS EOS. At finite temperature thermal pions occur, which also affect the chemical equilibrium but may overall stiffen the EOS for very high temperatures.

For isolated, cold NSs in neutrinoless beta-equilibrium, the inclusion of pions leads to a softening of the EOS compared to the respective model without pions. This affects the TOV solutions of NSs. The inclusion of pions leads to a decrease of the maximum mass of NSs and to smaller NS radii for a given mass. The magnitude of these effects is inversely related to the adopted pion mass. Radii decrease by at most  $\sim 200$  m for pion masses close to their vacuum value. For  $m_{\pi} = 200$  MeV models, changes of the stellar structure is very small since the condensation is largely suppressed.

The tidal deformability can change by about 10 percent for pion masses equal to their vacuum value. This might affect the EOS inference from a GW analysis study of the inspiral if microphysical parameters of nuclear matter are deduced using microphysical EOS models which neglect pions.

To understand the influence of pions on the BNS mergers, we conduct relativistic hydrodynamical simulations with the different EOS models with and without pions. We focus on  $1.35\text{-}1.35 M_{\odot}$  mergers but also simulate equal-mass binaries with higher total binary mass.

Concerning the general dynamics of the merger there are no qualitative differences comparing simulations with and without pions. However, we find that depending on the adopted pion mass the electron fraction can be significantly altered, albeit we employ a rather crude treatment of weak interactions by simply advecting the initial electron fraction. For a more sophisticated treatment

one should also include muons. We briefly estimate the potential impact of muons in the appendix. In essence, we find that if pions have a sizable impact on the stellar structure for effective pion masses close to the vacuum values, the changes by adding muons are relatively small. For most of our simulated binary configurations we find that pions in the condensate are more abundant than thermal pions. Only for high effective pion masses, thermal pions dominate in the postmerger phase.

We analyze the GW signal in our simulations and observe that the dominant postmerger GW frequency is shifted to higher frequencies by up to 200 Hz compared to the base model without pions. The shift is more pronounced for smaller effective pion masses. We evaluate how these changes compare to empirical relations between stellar parameters of NSs and the dominant postmerger frequency (e.g. [37, 38, 40–45, 47, 48, 50, 51]). These relations have been obtained in the literature considering large sets of EOS models that neglect pions. We find that these relations remain to good accuracy valid because the inclusion of pions changes both the properties of nonrotating NSs and of postmerger remnants. This justifies to use these relations for the EOS inference in GW observations. Only for small pion close to their vacuum values slight deviations may occur.

Similarly, we investigate the impact of pions on the threshold binary mass  $M_{\text{thres}}$  for prompt black-hole formation. Again, we find that the overall softening of the EOS compared to a base model without pions, leads to a reduction of  $M_{\text{thres}}$ . The reduction can be as large as about  $0.07 M_{\odot}$  and is more significant for small pion masses. Again, the inclusion of pions does not lead to significant deviations in empirical relations for  $M_{\text{thres}}$  which have been built using models without pions [52]. Similarly, we find relations for the maximum density in the early postmerger evolution to be fulfilled [50].

We also briefly assess the consequences for mass ejection in NS mergers. We find that the presence of pions leads to enhanced mass ejection by a few ten per cent compared to the base models. Also ejecta properties such as their mass have been related to stellar parameters of nonrotating NSs [90, 91]. In this respect we observe that the ejecta mass increase in our models with pions is stronger than one would naively expect based on the changes of stellar parameters of cold, nonrotating stars. This might indicate a systematic bias with consequences for attempts to infer stellar parameters from kilonova observations, but we caution that ejecta properties are generally challenging to resolve and that the uncertainties and the intrinsic scatter in relations describing kilonova features as function of NS properties are rather large.

Future research should improve this first assessment of pion effects in NS mergers in several ways. We describe pions as noninteracting Boson gas and choose a constant pion mass, which allows only a coarse description of the impact on the EOS. A more sophisticated treatment of weak interactions is desirable to understand the impact on the ejecta composition, where our crude simulations already indicate a potential influence as pions change the electron fraction. Clearly, more EOS models should be considered in future work.

### Appendix A: Impact of muons

In this study we focus on the impact that pions have on BNS. We do not consider muons, which we also neglected in many currently available EOS tables, although one should expect that also muons are present in NS matter (see [98–100] for the consideration of muons in simulations of core-collapse supernovae and NS mergers). The chemical potential of electrons can reach the rest mass of muons of 105.7 MeV, which can be seen in Fig. 11. Muons are the decay products of pions and should thus in principle be taken into account. We assess the influence of muons by considering stellar equilibrium solutions of isolated stars. We are mostly interested in the impact on the GW signal and the collapse behavior, both of which are determined primarily by the high-density regime of the EOS.

The consideration of muons in EOS tables is in principle straightforward as they can be treated as an ideal Fermi gas similar to electrons. Including muons in the existing tables requires some minor adaptations because the base models determine the contributions of the different constituents by assuming charge neutrality between protons, electrons and positrons. Adding muons and pions thus changes the conditions for charge neutrality. To this end we first remove the contributions from electrons (and positrons for  $T > 0$ ) from the base model as we did for adding pions. We then recalculate at every point of the EOS table the contributions of all considered leptons and pions considering the respective new relation for charge neutrality and chemical equilibrium. We consider stel-

lar configurations at zero temperature and neutrinoless  $\beta$ -equilibrium. Moreover, we investigate stellar models at finite temperature to mimic the behavior of merger remnants. For those we choose a finite temperature of 20 MeV and fix the lepton fraction. At every point of the EOS table with this temperature, we solve the conditions for charge neutrality under the assumption of chemical equilibrium between the nucleons, the leptons (electrons, muons, their anti-particles, and the respective neutrinos and anti-neutrinos), and the pions. We emphasize that this analysis is meant to estimate the impact on GWs and bulk properties of NSs and BNS mergers, which are mostly determined by the high-density EOS, where these conditions are well justified.

Following the aforementioned procedure we construct different versions of the EOS tables at zero temperature using the SFHo and DD2 base models: the base model with pions only, the base models with muons only, and the base model with muons and pions. For those we determine the beta-equilibrium EOS at zero temperature and compute TOV solutions, which are shown in Fig. 23 for SFHo (left panel) and DD2 (right panel). Here we only consider an effective pion mass which equals the vacuum mass.

The inclusion of muons without pions leads to a mild softening of the EOS and yields smaller NS radii. The softening induced by pions is in comparison more significant. For instance, the reduction of the radius and the maximum mass is more pronounced. Interestingly, we find that adding muons to an EOS with pions has only a negligible impact. This is understandable because in the presence of pions the difference  $\mu_n - \mu_p$  is limited by the pion mass. Hence, under the conditions of neutrinoless beta-equilibrium,  $\mu_n - \mu_p = \mu_e = \mu_\pi = \mu_\mu$ , the muon production is suppressed as  $\mu_\mu$  cannot grow a lot. One may thus argue that neglecting muons is a good approximation in our models with relatively small effective pion masses. However, for the models with higher effective pion mass the suppression of muons will be less restrictive. In this case the inclusion of pions has not a strong impact on the EOS (see Sect. IV A), but modifications by muons may become somewhat more significant (see the case where we consider only muons and the base model).

A similar picture arises for finite-temperature EOS models, where we also consider neutrinos (see Fig. 24). We fix the electronic lepton fraction to  $Y_{\text{lep},e} = 0.04$  and the muonic lepton fraction to  $Y_{\text{lep},\mu} = 0.015$  (if muon and muon neutrinos are present), which is coarsely representative of BNS merger remnants. Here, we assume that the initial electronic and muonic lepton fractions of the original cold neutron stars are approximately preserved during the merger at the high densities considered here due to neutrino-trapping. To better assess the impact on the stellar structure, we compute TOV models for which we disregard densities below  $10^{14}$  g/cm<sup>3</sup>, i.e. we define the surface of such models to be at this density. In this way, we avoid that the stellar models are inflated by the

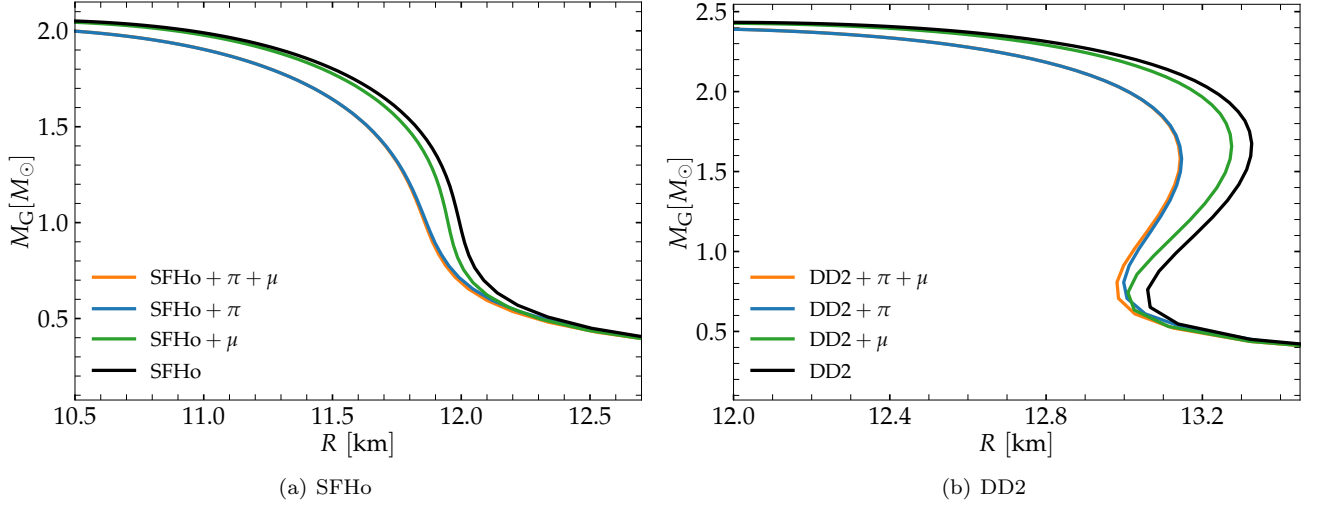


FIG. 23. Gravitational mass versus NS radius for the Base, Base+ $\pi$ , Base+ $\mu$  and Base+ $\pi$ + $\mu$  models with SFHo(left) and DD2(right) as base model.

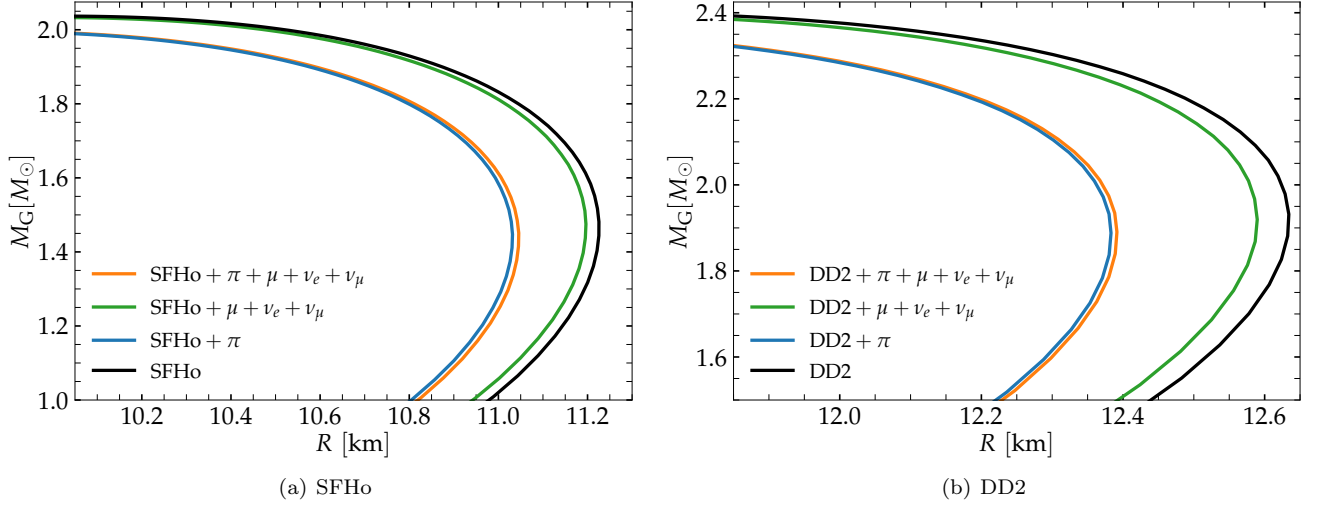


FIG. 24. Gravitational mass versus NS radius for the Base, Base+ $\pi$ , Base+ $\mu$ + $\nu_e$ + $\nu_\mu$ , Base+ $\pi$ + $\mu$ + $\nu_e$ + $\nu_\mu$  for a fixed electronic lepton fraction  $Y_{\text{lep},e} = 0.04$ , and muonic lepton fraction  $Y_{\text{lep},\mu} = 0.015$  (if muon and muon neutrinos are present) at temperature  $T = 20$  MeV with SFHo(left) and DD2(right) as base models. For these calculations the surface of the stars is defined at a rest-mass density of  $10^{14}$  g/cm<sup>3</sup>.

finite temperature at lower densities.

Again, we find that the impact of muons is nearly negligible if pions are included as can be seen by comparing the blue and orange lines in Fig. 24. The comparison between the different EOS versions also reveals that ignoring neutrinos in our analysis can be justified as they apparently have only a small influence on the stellar structure. We thus conclude that considering only pions and ignoring muons in the BNS merger simulations discussed in the main text is a reasonable approximation for a first study evaluating the bulk properties of mergers like GWs and the conditions for black-hole formation.

## ACKNOWLEDGMENTS

We thank Bengt Friman, Pok Man Lo and Jochen Wambach for helpful discussions. VV and AB acknowledge support by Deutsche Forschungsgemeinschaft (DFG, German Research Foundation) - Project-ID 138713538 - SFB 881 (“The Milky Way System”, subproject A10). NR and GMP acknowledge support by the European Research Council (ERC) under the European Union’s Horizon 2020 research and innovation program (ERC Advanced Grant KILONOVA No. 885281). AB acknowledges by the European Research Council (ERC) under the European Union’s Horizon 2020 research and

innovation program under grant agreement No. 759253. AB, GMP, ILA and NR acknowledge support by DFG

- Project-ID 279384907 - SFB 1245. AB and GMP acknowledge support by the State of Hesse within the Cluster Project ELEMENTS.

- 
- [1] R. Fernández and B. D. Metzger, Electromagnetic Signatures of Neutron Star Mergers in the Advanced LIGO Era, *Annu. Rev. Nucl. Part. Sci.* **66**, 23 (2016).
- [2] L. Baiotti and L. Rezzolla, Binary neutron star mergers: a review of Einstein’s richest laboratory, *Rep. Prog. Phys.* **80**, 096901 (2017).
- [3] M. Shibata and K. Hotokezaka, Merger and Mass Ejection of Neutron Star Binaries, *Annu. Rev. Nucl. Part. Sci.* **69**, 41 (2019).
- [4] B. D. Metzger, Kilonovae, *Living Reviews in Relativity* **23**, 1 (2019).
- [5] A. Bauswein and N. Stergioulas, Spectral classification of gravitational-wave emission and equation of state constraints in binary neutron star mergers, *J. Phys. G: Nucl. Part. Phys.* **46**, 113002 (2019).
- [6] D. Radice, S. Bernuzzi, and A. Perego, The Dynamics of Binary Neutron Star Mergers and GW170817, *Annu. Rev. Nucl. Part. Sci.* **70**, 95 (2020).
- [7] E. Nakar, The electromagnetic counterparts of compact binary mergers, *Phys. Rep.* **886**, 1 (2020).
- [8] K. Chatziioannou, Neutron-star tidal deformability and equation-of-state constraints, *Gen. Relativ. Gravit.* **52**, 109 (2020).
- [9] J. J. Cowan, C. Sneden, J. E. Lawler, A. Aprahamian, M. Wiescher, K. Langanke, G. Martínez-Pinedo, and F.-K. Thielemann, Origin of the heaviest elements: The rapid neutron-capture process, *Rev. Mod. Phys.* **93**, 015002 (2021).
- [10] T. Dietrich, T. Hinderer, and A. Samajdar, Interpreting binary neutron star mergers: describing the binary neutron star dynamics, modelling gravitational waveforms, and analyzing detections, *Gen. Relativ. Gravit.* **53**, 27 (2021).
- [11] S. Rosswog and O. Korobkin, Heavy elements and electromagnetic transients from neutron star mergers, arXiv e-prints (2022), [arXiv:2208.14026](https://arxiv.org/abs/2208.14026) [astro-ph.HE].
- [12] H. T. Janka and A. Bauswein, Dynamics and Equation of State Dependencies of Relevance for Nucleosynthesis in Supernovae and Neutron Star Mergers, arXiv e-prints (2022), [arXiv:2212.07498](https://arxiv.org/abs/2212.07498) [astro-ph.HE].
- [13] J. M. Lattimer, The Nuclear Equation of State and Neutron Star Masses, *Annu. Rev. Nucl. Part. Sci.* **62**, 485 (2012).
- [14] M. Oertel, M. Hempel, T. Klähn, and S. Typel, Equations of state for supernovae and compact stars, *Rev. Mod. Phys.* **89**, 015007 (2017).
- [15] G. Baym, T. Hatsuda, T. Kojo, P. D. Powell, Y. Song, and T. Takatsuka, From hadrons to quarks in neutron stars: a review, *Rep. Prog. Phys.* **81**, 056902 (2018).
- [16] A. R. Raduta, F. Nacu, and M. Oertel, Equations of state for hot neutron stars, *Eur. Phys. J. A* **57**, 329 (2021).
- [17] J. Piekarewicz, The Nuclear Physics of Neutron Stars, arXiv e-prints (2022), [arXiv:2209.14877](https://arxiv.org/abs/2209.14877) [nucl-th].
- [18] A. R. Raduta, Equations of state for hot neutron stars-II. The role of exotic particle degrees of freedom, *Eur. Phys. J. A* **58**, 115 (2022).
- [19] J. Keller, K. Hebeler, and A. Schwenk, Nuclear equation of state for arbitrary proton fraction and temperature based on chiral effective field theory and a Gaussian process emulator, arXiv e-prints (2022), [arXiv:2204.14016](https://arxiv.org/abs/2204.14016) [nucl-th].
- [20] R. F. Sawyer, Condensed  $\pi^-$  Phase in Neutron-Star Matter, *Phys. Rev. Lett.* **29**, 382 (1972).
- [21] A. B. Migdal, Phase transitions ( $\pi$ -condensation) in nuclei and neutron stars, *Physics Letters B* **45**, 448 (1973).
- [22] G. Baym and E. Flowers, Pion condensation in neutron star matter: Equilibrium conditions and model calculations, *Nucl. Phys. A* **222**, 29 (1974).
- [23] W. Weise and G. E. Brown, Equation of state for neutron matter in the presence of a pion condensate, *Physics Letters B* **58**, 300 (1975).
- [24] S. O. Bäckman and W. Weise, Calculation of the threshold for  $\pi^-$  condensation in neutron matter, *Physics Letters B* **55**, 1 (1975).
- [25] A. B. Migdal, Pion fields in nuclear matter, *Rev. Mod. Phys.* **50**, 107 (1978).
- [26] T. Ericson and W. Weise, *Pions and nuclei*, The International series of monographs on physics No. 74 (Oxford University Press, New York, 1988).
- [27] A. B. Migdal, E. E. Saperstein, M. A. Troitsky, and D. N. Voskresensky, Pion degrees of freedom in nuclear matter, *Phys. Rep.* **192**, 179 (1990).
- [28] A. Akmal and V. R. Pandharipande, Spin-isospin structure and pion condensation in nucleon matter, *Phys. Rev. C* **56**, 2261 (1997).
- [29] R. W. Mayle, M. Tavani, and J. R. Wilson, Pions, Supernovae, and the Supranuclear Matter Density Equation of State, *Astrophys. J.* **418**, 398 (1993).
- [30] C. Ishizuka, A. Ohnishi, K. Tsubakihara, K. Sumiyoshi, and S. Yamada, Tables of hyperonic matter equation of state for core-collapse supernovae, *J. Phys. G: Nucl. Part. Phys.* **35**, 085201 (2008).
- [31] K. Nakazato, K. Sumiyoshi, and S. Yamada, Astrophysical implications of equation of state for hadron-quark mixed phase: Compact stars and stellar collapses, *Phys. Rev. D* **77**, 103006 (2008).
- [32] K. Nakazato, K. Sumiyoshi, and S. Yamada, Impact of Quarks and Pions on Dynamics and Neutrino Signal of Black Hole Formation in Non-rotating Stellar Core Collapse, *Astrophys. J.* **721**, 1284 (2010).
- [33] M. Oertel, A. F. Fantina, and J. Novak, Extended equation of state for core-collapse simulations, *Phys. Rev. C* **85**, 055806 (2012).
- [34] B. Peres, M. Oertel, and J. Novak, Influence of pions and hyperons on stellar black hole formation, *Phys. Rev. D* **87**, 043006 (2013).
- [35] B. Fore and S. Reddy, Pions in hot dense matter and their astrophysical implications, *Phys. Rev. C* **101**, 035809 (2020).
- [36] A. S. Schneider, C. Constantinou, B. Muccioli, and M. Prakash, Akmal-Pandharipande-Ravenhall equation

- of state for simulations of supernovae, neutron stars, and binary mergers, *Phys. Rev. C* **100**, 025803 (2019).
- [37] A. Bauswein and H. T. Janka, Measuring Neutron-Star Properties via Gravitational Waves from Neutron-Star Mergers, *Phys. Rev. Lett.* **108**, 011101 (2012).
- [38] A. Bauswein, H.-T. Janka, K. Hebeler, and A. Schwenk, Equation-of-state dependence of the gravitational-wave signal from the ring-down phase of neutron-star mergers, *Phys. Rev. D* **86**, 063001 (2012).
- [39] A. Bauswein, T. W. Baumgarte, and H. T. Janka, Prompt Merger Collapse and the Maximum Mass of Neutron Stars, *Phys. Rev. Lett.* **111**, 131101 (2013).
- [40] K. Hotokezaka, K. Kiuchi, K. Kyutoku, T. Muranushi, Y.-i. Sekiguchi, M. Shibata, and K. Taniguchi, Remnant massive neutron stars of binary neutron star mergers: Evolution process and gravitational waveform, *Phys. Rev. D* **88**, 044026 (2013).
- [41] A. Bauswein, N. Stergioulas, and H. T. Janka, Revealing the high-density equation of state through binary neutron star mergers, *Phys. Rev. D* **90**, 023002 (2014).
- [42] S. Bernuzzi, T. Dietrich, and A. Nagar, Modeling the Complete Gravitational Wave Spectrum of Neutron Star Mergers, *Phys. Rev. Lett.* **115**, 091101 (2015).
- [43] K. Takami, L. Rezzolla, and L. Baiotti, Spectral properties of the post-merger gravitational-wave signal from binary neutron stars, *Phys. Rev. D* **91**, 064001 (2015).
- [44] L. Rezzolla and K. Takami, Gravitational-wave signal from binary neutron stars: A systematic analysis of the spectral properties, *Phys. Rev. D* **93**, 124051 (2016).
- [45] L. Lehner, S. L. Liebling, C. Palenzuela, O. L. Caballero, E. O'Connor, M. Anderson, and D. Neilsen, Unequal mass binary neutron star mergers and multimessenger signals, *Class. Quantum Grav.* **33**, 184002 (2016).
- [46] S. Köppel, L. Bovard, and L. Rezzolla, A General-relativistic Determination of the Threshold Mass to Prompt Collapse in Binary Neutron Star Mergers, *Astrophys. J. Lett.* **872**, L16 (2019).
- [47] M. Breschi, S. Bernuzzi, F. Zappa, M. Agathos, A. Perego, D. Radice, and A. Nagar, Kilohertz gravitational waves from binary neutron star remnants: Time-domain model and constraints on extreme matter, *Phys. Rev. D* **100**, 104029 (2019).
- [48] K. W. Tsang, T. Dietrich, and C. Van Den Broeck, Modeling the postmerger gravitational wave signal and extracting binary properties from future binary neutron star detections, *Phys. Rev. D* **100**, 044047 (2019).
- [49] M. Agathos, F. Zappa, S. Bernuzzi, A. Perego, M. Breschi, and D. Radice, Inferring prompt black-hole formation in neutron star mergers from gravitational-wave data, *Phys. Rev. D* **101**, 044006 (2020).
- [50] S. Blacker, N.-U. F. Bastian, A. Bauswein, D. B. Blaschke, T. Fischer, M. Oertel, T. Soutanis, and S. Typel, Constraining the onset density of the hadron-quark phase transition with gravitational-wave observations, *Phys. Rev. D* **102**, 123023 (2020).
- [51] S. Vretinaris, N. Stergioulas, and A. Bauswein, Empirical relations for gravitational-wave asteroseismology of binary neutron star mergers, *Phys. Rev. D* **101**, 084039 (2020).
- [52] A. Bauswein, S. Blacker, G. Lioutas, T. Soutanis, V. Vijayan, and N. Stergioulas, Systematics of prompt black-hole formation in neutron star mergers, *Phys. Rev. D* **103**, 123004 (2021).
- [53] S. D. Tootle, L. J. Papenfort, E. R. Most, and L. Rezzolla, Quasi-universal Behavior of the Threshold Mass in Unequal-mass, Spinning Binary Neutron Star Mergers, *Astrophys. J. Lett.* **922**, L19 (2021).
- [54] R. Kashyap, A. Das, D. Radice, S. Padamata, A. Prakash, D. Logoteta, A. Perego, D. A. Godzieba, S. Bernuzzi, I. Bombaci, F. J. Fattoyev, B. T. Reed, and A. d. S. Schneider, Numerical relativity simulations of prompt collapse mergers: Threshold mass and phenomenological constraints on neutron star properties after GW170817, *Phys. Rev. D* **105**, 103022 (2022).
- [55] M. Kölsch, T. Dietrich, M. Ujevic, and B. Brügmann, Investigating the mass-ratio dependence of the prompt-collapse threshold with numerical-relativity simulations, *Phys. Rev. D* **106**, 044026 (2022).
- [56] A. Akmal, V. R. Pandharipande, and D. G. Ravenhall, Equation of state of nucleon matter and neutron star structure, *Phys. Rev. C* **58**, 1804 (1998).
- [57] R. Rapp and J. Wambach, Equation of state of an interacting pion gas with realistic  $\pi$ - $\pi$  interactions, *Phys. Rev. C* **53**, 3057 (1996).
- [58] C. Jung, F. Rennecke, R.-A. Tripolt, L. von Smekal, and J. Wambach, In-medium spectral functions of vector- and axial-vector mesons from the functional renormalization group, *Phys. Rev. D* **95**, 036020 (2017).
- [59] R.-A. Tripolt, C. Jung, L. von Smekal, and J. Wambach, Vector and axial-vector mesons in nuclear matter, *Phys. Rev. D* **104**, 054005 (2021).
- [60] B. Fore and S. Reddy, Pions in hot dense matter and their astrophysical implications, *Phys. Rev. C* **101**, 035809 (2020).
- [61] B. Fore, N. Kaiser, S. Reddy, and N. C. Warrington, The mass of charged pions in neutron star matter, arXiv e-prints (2023), arXiv:2301.07226 [nucl-th].
- [62] M. Hempel and J. Schaffner-Bielich, A statistical model for a complete supernova equation of state, *Nuclear Physics A* **837**, 210 (2010).
- [63] M. Hempel, T. Fischer, J. Schaffner-Bielich, and M. Liebendörfer, New Equations of State in Simulations of Core-collapse Supernovae, *Astrophys. J.* **748**, 70 (2012).
- [64] A. W. Steiner, M. Hempel, and T. Fischer, Core-collapse Supernova Equations of State Based on Neutron Star Observations, *Astrophys. J.* **774**, 17 (2013).
- [65] S. Typel, Relativistic model for nuclear matter and atomic nuclei with momentum-dependent self-energies, *Phys. Rev. C* **71**, 064301 (2005).
- [66] S. Typel, G. Röpke, T. Klähn, D. Blaschke, and H. H. Wolter, Composition and thermodynamics of nuclear matter with light clusters, *Phys. Rev. C* **81**, 015803 (2010).
- [67] P.A. Zyla, et al. (Particle Data Group), Review of Particle Physics, *Progress of Theoretical and Experimental Physics* **2020**, 083C01 (2020).
- [68] H. Nishihara and M. Harada, Equation of state in the pion condensation phase in asymmetric nuclear matter using a holographic QCD model, *Phys. Rev. D* **90**, 115027 (2014).
- [69] P. M. Lo, B. Friman, M. Marczenko, K. Redlich, and C. Sasaki, Repulsive interactions and their effects on the thermodynamics of a hadron gas, *Phys. Rev. C* **96**, 015207 (2017).
- [70] Y. Sekiguchi, K. Kiuchi, K. Kyutoku, M. Shibata, and K. Taniguchi, Dynamical mass ejection from the

- merger of asymmetric binary neutron stars: Radiation-hydrodynamics study in general relativity, *Phys. Rev. D* **93**, 124046 (2016).
- [71] F. Foucart, R. Haas, M. D. Duez, E. O'Connor, C. D. Ott, L. Roberts, L. E. Kidder, J. Lippuner, H. P. Pfeiffer, and M. A. Scheel, Low mass binary neutron star mergers: Gravitational waves and neutrino emission, *Phys. Rev. D* **93**, 044019 (2016).
- [72] D. Radice, A. Perego, K. Hotokezaka, S. A. Fromm, S. Bernuzzi, and L. F. Roberts, Binary Neutron Star Mergers: Mass Ejection, Electromagnetic Counterparts, and Nucleosynthesis, *Astrophys. J.* **869**, 130 (2018).
- [73] R. Ardevol-Pulpillo, H.-T. Janka, O. Just, and A. Bauswein, Improved leakage-equilibration-absorption scheme (ILEAS) for neutrino physics in compact object mergers, *Mon. Not. Roy. Astron. Soc.* **485**, 4754 (2019).
- [74] R. C. Tolman, Static Solutions of Einstein's Field Equations for Spheres of Fluid, *Phys. Rev.* **55**, 364 (1939).
- [75] J. R. Oppenheimer and G. M. Volkoff, On Massive Neutron Cores, *Phys. Rev.* **55**, 374 (1939).
- [76] P. Haensel, A. Y. Potekhin, and D. G. Yakovlev, eds., *Neutron Stars 1: Equation of State and Structure*, Astrophysics and Space Science Library, Vol. 326 (Springer, New York, 2007).
- [77] J. M. Lattimer, Constraints on nuclear symmetry energy parameters, *Particles* **6**, 30 (2023).
- [78] J. Isenberg and J. Nester, Canonical Gravity, in *General Relativity and Gravitation. Vol. 1. One hundred years after the birth of Albert Einstein. Edited by A. Held. New York*, Vol. 1 (1980) p. 23.
- [79] J. R. Wilson, G. J. Mathews, and P. Marronetti, Relativistic numerical model for close neutron-star binaries, *Phys. Rev. D* **54**, 1317 (1996).
- [80] R. Oechslin, S. Rosswog, and F.-K. Thielemann, Conformally flat smoothed particle hydrodynamics application to neutron star mergers, *Phys. Rev. D* **65**, 103005 (2002).
- [81] R. Oechslin, H.-T. Janka, and A. Marek, Relativistic neutron star merger simulations with non-zero temperature equations of state, *Astron. & Astrophys.* **467**, 395 (2007).
- [82] A. Bauswein, R. Oechslin, and H. T. Janka, Discriminating strange star mergers from neutron star mergers by gravitational-wave measurements, *Phys. Rev. D* **81**, 024012 (2010).
- [83] T. Hinderer, Tidal Love Numbers of Neutron Stars, *Astrophys. J.* **677**, 1216 (2008).
- [84] K. Chatziioannou, J. A. Clark, A. Bauswein, M. Millhouse, T. B. Littenberg, and N. Cornish, Inferring the post-merger gravitational wave emission from binary neutron star coalescences, *Phys. Rev. D* **96**, 124035 (2017).
- [85] G. Lioutas, A. Bauswein, and N. Stergioulas, Frequency deviations in universal relations of isolated neutron stars and postmerger remnants, *Phys. Rev. D* **104**, 043011 (2021).
- [86] A. Bauswein, N.-U. F. Bastian, D. B. Blaschke, K. Chatziioannou, J. A. Clark, T. Fischer, and M. Oertel, Identifying a First-Order Phase Transition in Neutron-Star Mergers through Gravitational Waves, *Phys. Rev. Lett.* **122**, 061102 (2019).
- [87] A. Bauswein, S. Blacker, V. Vijayan, N. Stergioulas, K. Chatziioannou, J. A. Clark, N.-U. F. Bastian, D. B. Blaschke, M. Cierniak, and T. Fischer, Equation of State Constraints from the Threshold Binary Mass for Prompt Collapse of Neutron Star Mergers, *Phys. Rev. Lett.* **125**, 141103 (2020).
- [88] A. Bauswein, O. Just, H.-T. Janka, and N. Stergioulas, Neutron-star Radius Constraints from GW170817 and Future Detections, *Astrophys. J. Lett.* **850**, L34 (2017).
- [89] A. Bauswein, N.-U. F. Bastian, D. Blaschke, K. Chatziioannou, J. A. Clark, T. Fischer, H.-T. Janka, O. Just, M. Oertel, and N. Stergioulas, Equation-of-state constraints and the QCD phase transition in the era of gravitational-wave astronomy, *AIP Conference Proceedings* **2127**, 020013 (2019).
- [90] A. Bauswein, S. Goriely, and H. T. Janka, Systematics of Dynamical Mass Ejection, Nucleosynthesis, and Radioactively Powered Electromagnetic Signals from Neutron-star Mergers, *Astrophys. J.* **773**, 78 (2013).
- [91] K. Hotokezaka, K. Kiuchi, K. Kyutoku, H. Okawa, Y.-i. Sekiguchi, M. Shibata, and K. Taniguchi, Mass ejection from the merger of binary neutron stars, *Phys. Rev. D* **87**, 024001 (2013).
- [92] T. Dietrich and M. Ujevic, Modeling dynamical ejecta from binary neutron star mergers and implications for electromagnetic counterparts, *Class. Quantum Grav.* **34**, 105014 (2017).
- [93] M. W. Coughlin, T. Dietrich, Z. Doctor, D. Kasen, S. Coughlin, A. Jerkstrand, G. Leloudas, O. McBrien, B. D. Metzger, R. O'Shaughnessy, and S. J. Smartt, Constraints on the neutron star equation of state from AT2017gfo using radiative transfer simulations, *Mon. Not. Roy. Astron. Soc.* **480**, 3871 (2018).
- [94] C. J. Krüger and F. Foucart, Estimates for disk and ejecta masses produced in compact binary mergers, *Phys. Rev. D* **101**, 103002 (2020).
- [95] V. Nedora, F. Schianchi, S. Bernuzzi, D. Radice, B. Daszuta, A. Endrizzi, A. Perego, A. Prakash, and F. Zappa, Mapping dynamical ejecta and disk masses from numerical relativity simulations of neutron star mergers, *Class. Quantum Grav.* **39**, 015008 (2021).
- [96] O. Just, S. Goriely, H. T. Janka, S. Nagataki, and A. Bauswein, Neutrino absorption and other physics dependencies in neutrino-cooled black hole accretion discs, *Mon. Not. R. Astron. Soc.* **509**, 1377 (2022).
- [97] T. Dietrich, M. W. Coughlin, P. T. H. Pang, M. Bulla, J. Heinzel, L. Issa, I. Tews, and S. Antier, Multimesenger constraints on the neutron-star equation of state and the Hubble constant, *Science* **370**, 1450 (2020).
- [98] R. Bollig, H.-T. Janka, A. Lohs, G. Martínez-Pinedo, C. J. Horowitz, and T. Melson, Muon creation in supernova matter facilitates neutrino-driven explosions, *Phys. Rev. Lett.* **119**, 242702 (2017).
- [99] E. Loffredo, A. Perego, D. Logoteta, and M. Branchesi, Muons in the aftermath of Neutron Star Mergers and their impact on Trapped Neutrinos, arXiv e-prints (2022), arXiv:2209.04458 [astro-ph.HE].
- [100] M. Alford, A. Harutyunyan, and A. Sedrakian, Bulk Viscosity of Relativistic  $npe\mu$  Matter in Neutron-Star Mergers, *Particles* **5**, 361 (2022).